Monthly Notices of the ROYAL ASTRONOMICAL SOCIETY

Mon. Not. R. Astron. Soc. **417,** 2144–2160 (2011) doi:10.1111/j.1365-2966.2011.19397.x

X-ray flare candidates in short gamma-ray bursts

R. Margutti,[1,2★] G. Chincarini,[1,3] J. Granot,[4,5,6] C. Guidorzi,[7] E. Berger,[2] M. G. Bernardini,[1] N. Gehrels,[8] A. M. Soderberg,[2] M. Stamatikos[8,9] and E. Zaninoni[1,10]

[1]*INAF Osservatorio Astronomico di Brera, via Bianchi 46, Merate 23807, Italy*
[2]*Harvard-Smithsonian Center for Astrophysics, 60 Garden Street, Cambridge, MA 02138, USA*
[3]*Univerisitá Milano Bicocca, Dip. Fisica G. Occhialini, P.zza della Scienza 3, Milano 20126, Italy*
[4]*Racah Institute of Physics, The Hebrew University, Jerusalem 91904, Israel*
[5]*Raymond and Beverly Sackler School of Physics & Astronomy, Tel Aviv University, Tel Aviv 69978, Israel*
[6]*Centre for Astrophysics Research, University of Hertfordshire, College Lane, Hatfield, Herts AL10 9AB*
[7]*Physics Department, University of Ferrara, via Saragat 1, I-44122 Ferarra, Italy*
[8]*NASA-Goddard Space Flight Center, Greenbelt, MD 20771, USA*
[9]*Department of Physics and Center for Cosmology and Astro-Particle Physics, Ohio State University, Columbus, OH 43210, USA*
[10]*Univerisitá di Padova, Dip. Astronomia, v. dell' Osservatorio 31, Padova 35122, Italy*

Accepted 2011 July 6. Received 2011 June 16; in original form 2011 April 29

ABSTRACT

We present the first systematic study of X-ray flare candidates in short gamma-ray bursts (SGRBs) exploiting the large 6-year *Swift* data base with the aim to constrain the physical nature of such fluctuations. We find that flare candidates appear in different types of SGRB host galaxy environments and show no clear correlation with the X-ray afterglow lifetime; flare candidates are detected both in SGRBs with a bright extended emission in the soft γ-rays and in SGRBs which do not show such component. We furthermore show that SGRB X-ray flare candidates only *partially* share the set of observational properties of long GRB (LGRB) flares. In particular, the main parameter driving the duration evolution of X-ray variability episodes in both classes is found to be the elapsed time from the explosion, with very limited dependence on the different progenitors, environments, central engine lifetimes, prompt variability time-scales and energy budgets. On the contrary, SGRB flare candidates significantly differ from LGRB flares in terms of peak luminosity, isotropic energy, flare-to-prompt luminosity ratio and relative variability flux. However, these differences disappear when the central engine time-scales and energy budget are accounted for, suggesting that (i) flare candidates and prompt pulses in SGRBs likely have a common origin; (ii) similar dissipation and/or emission mechanisms are responsible for the prompt and flare emission in LGRBs and SGRBs, with SGRBs being less energetic albeit faster evolving versions of the long class. Finally, we show that in strict analogy to the SGRB prompt emission, flares candidates fall off the lag–luminosity relation defined by LGRBs, thus strengthening the SGRB flare–prompt pulse connection.

Key words: radiation mechanisms: non-thermal – gamma-ray burst: general.

1 INTRODUCTION

With an isotropic peak luminosity up to 10^{54} erg s^{-1}, gamma-ray bursts (GRBs) are the brightest objects in the γ-ray sky during their short lives ($\Delta t \sim 0.1$–100 s). Their duration–spectral hardness distribution gives evidence for the presence of two classes (Kouveliotou et al. 1993): long GRBs (LGRBs) and short GRBs (SGRBs; observed duration longer and shorter than 2 s, respectively), with short bursts appearing slightly harder. The dichotomy in the duration–hardness dimensions suggested separate progenitor populations. However, until a few years ago, the distances, energy and environments of SGRBs remained highly uncertain due to the poor localization.

The breakthrough in the study of SGRBs occurred thanks to the rapid slew capabilities of the *Swift* spacecraft (Gehrels et al. 2004) which allowed spectroscopic observations to be performed at very early times. These observations revealed that SGRBs are cosmological, with prompt luminosities comparable to LGRBs albeit significantly less energetic; with similar afterglows (Nysewander, Fruchter & Pe'er 2009) but residing in completely different environments. In sharp contrast to LGRBs, short bursts have been localized both in early-type and late-type host galaxies (see Berger 2011 and

★E-mail: raffaella.margutti@brera.inaf.it

© 2011 The Authors
Monthly Notices of the Royal Astronomical Society © 2011 RAS

Downloaded from http://mnras.oxfordjournals.org/ at NASA Goddard Space Flight Ctr on July 11, 2014

references therein), pointing to an *old* progenitor population. The detection of supernovae associated to LGRBs (see e.g. Kulkarni et al. 1998; Stanek et al. 2003; Fruchter et al. 2006 and references therein) provided instead support to models invoking *young* stellar progenitors. According to the standard scenario, LGRBs originate from the collapse of rapidly rotating, massive stars (MacFadyen & Woosley 1999), while SGRBs are believed to result from the coalescence of a binary system of compact objects (neutron star plus neutron star, NS+NS, or neutron star plus black hole, NS+BH; Paczynski 1986; Eichler et al. 1989; Narayan, Paczynski & Piran 1992).

Despite fundamental theoretical and observational progress, the nature of SGRB progenitors remains elusive. Numerical simulations show that the active stage of a NS+NS merger typically lasts ∼(0.01–0.1) s (see e.g. Nakar 2007 and references therein)[1]: material ejected during the merger is expected to accrete on time-scales of the order of 1–10 s (the exact value depending on the accreting disc viscosity parameter and details of the ejection process). Thus, the detection of central engine activity on time-scales much longer than the usual dynamical or even viscous time-scales would challenge the currently accepted scenario (see Nakar 2007, for a recent review).

Long-lasting ($\Delta t \gg 10$ s), soft energy tails detected in several SGRBs during their prompt emission (the so-called extended emission; see Norris, Gehrels & Scargle 2010a and references therein) represent such a case and pose severe constraints to existing models, especially when energetically dominating with respect to the primary burst (Perley et al. 2009). The same is true for the recently discovered presence of precursors (Troja, Rosswog & Gehrels 2010). Equally challenging would be the detection of late-time central engine activity in the form of *flares* superimposed over the smooth SGRB X-ray afterglow.

Flares are currently detected in ∼30 per cent of *long* GRBs X-ray afterglows (Chincarini et al. 2010) as fast-rise exponential-decay features whose spectral and temporal properties have been demonstrated to show a strict analogy to LGRB prompt pulses (Margutti et al. 2010b): this finding suggested that flares might originate from re-activations of the LGRB central engine. Several ideas on how to explain the possible presence of flares in *short* GRBs have been explored as well: the fragmentation of the outer parts of an hyperaccreting disc around the newly formed black hole as a result of gravitational instabilities could potentially lead to large-amplitude variations of the central engine output of both LGRBs and SGRBs (Perna, Armitage & Zhang 2006). Alternatively, the late-time accretion of material launched into eccentric but gravitationally bound orbits during the compact binary merger could provide the fuel to revive the central engine activity (Rosswog 2007). The long-term evolution of debris following the tidal disruption of compact objects has been identified by Lee, Ramirez-Ruiz & L-pez-Cmara (2009) as a feasible mechanism to produce flares. Finally, as an alternative in the context of accretion-powered models, magnetic halting may also give rise to secondary episodes of delayed activity as suggested by Proga & Zhang (2006). However, the observational properties of flares in SGRBs have not been determined, yet, so that it is at the moment unclear if any of these models would be able to explain the observations.

While SGRB X-ray light curves clearly show temporal variability superimposed over a smooth decay, the presence of real flares in short bursts is questionable. In particular, it is at the moment unclear if what is currently identified as SGRB flare emission (see e.g. La Parola et al. 2006 for GRB 051210) quantitatively shares the very same properties of the population of LGRB flares: are there fast varying $\Delta t/t \ll 1$, prominent temporal features in the afterglow of SGRBs with properties reminiscent of the LGRB flaring emission? Do SGRB flare *candidates* follow the entire set of relations found from the analysis of real flares in long bursts? In particular: is the evolution of their temporal and energetic properties compatible with the flare-like behaviour identified by Chincarini et al. (2010)? What is the typical amount of energy released during such episodes of variability? Is there any link between the late-time variability which appears in the X-ray afterglow of SGRBs and their prompt emission? Negligible spectral lag is a defining characteristic of SGRB prompt pulses: is this picture still valid when considering their late-time variability?

Prompted by this set of still open questions, we present the first systematic study of X-ray flare candidates in SGRBs, taking advantage from the large *Swift* 6-year data base. Through a homogeneous temporal and spectral analysis of the widest sample of SGRB light curves available at the time of writing, this study allows us to perform a one-to-one comparison with the properties of X-ray flares detected in long bursts (Chincarini et al. 2010; Margutti et al. 2010b, 2011; Bernardini et al. 2011). The primary goal of this paper is to observationally constrain the origin of SGRB flare candidates providing the reader with a complete picture of their properties.

This work is organized as follows. The sample selection and data reduction is presented in Section 2. Results are described in Section 3 and discussed in Section 4. Conclusions are drawn in Section 5.

The GRB phenomenology is presented in the observer frame. Isotropic equivalent luminosities and energies are listed. The observer frame 0.3–10 keV energy band is adopted unless specified. The zero time is assumed to be the trigger time. We use the notation: $Y_{\rm F}^{\rm SGRB}$ ($Y_{\rm P}^{\rm LGRB}$) to indicate that Y refers to the flare (prompt) emission of SGRBs (LGRBs). All the quoted uncertainties are given at 68 per cent confidence level (c.l.). Standard cosmological quantities have been adopted: $H_0 = 70\,{\rm km\,s^{-1}\,Mpc^{-1}}$, $\Omega_\Lambda = 0.7$, $\Omega_{\rm M} = 0.3$.

2 SAMPLE SELECTION AND DATA ANALYSIS

We select the SGRBs detected by the *Swift*-Burst Alert Telescope (BAT; Barthelmy et al. 2005a) and promptly repointed by the *Swift*-X-Ray Telescope (XRT; Burrows et al. 2005) between 2005 April and 2011 February. The short nature of each event is established using the combined information from the duration, hardness and spectral lag of its prompt γ-ray emission: a prompt γ-ray duration $T_{90} \lesssim 2$ s coupled to a hard γ-ray emission with photon index $\Gamma \lesssim 1.5$ and a negligible γ-ray spectral lag $\tau_{\rm lag}^{\gamma}$ are considered indicative of a SGRB nature (see Table 1). The morphology of the host galaxy is also used as an additional indicator, when available. The final sample comprises 60 SGRBs. The presence of X-ray variability in each SGRB is investigated following the method by Margutti et al. (2011), used to determine the presence of flares in LGRBs. Only GRBs showing fluctuations with a minimum 2σ[2] significance with respect to the continuum have been considered in the following analysis. This procedure automatically identifies the best time intervals to be searched for the presence of X-ray flare candidates in SGRBs. Out of ∼60 *Swift* SGRBs, eight satisfy the variability

[1] In a recent study Rezzolla et al. (2011) found $\Delta t \sim 0.3$ s.

[2] A 3σ threshold would only exclude GRB 051210, where the fluctuation has a significance of $\sim 2.8\sigma$.

Downloaded from http://mnras.oxfordjournals.org/ at NASA Goddard Space Flight Ctr on July 11, 2014

Table 1. X-ray and γ-ray properties for the sample of SGRBs analysed in this work. From left to right: GRB name: a (*) indicates an early-type host galaxy morphology (Fong et al. 2010, 2011), while GRBs with detected extended emission are in boldface; redshift, duration and average spectral photon index of the prompt 15–150 keV emission as determined from GCNs; EE duration and EE to IPC intensity ratio ($R_{\rm int}$) from Norris et al. (2010a): upper limits on $R_{\rm int}$ are listed when no EE has been detected (EE with zero duration); $t_{\rm i}$ and $t_{\rm f}$ define the temporal window for the X-ray lag calculation while the $\Delta t_{\rm reb}$ column reports the time-scale used to rebin the X-ray light-curve pairs; CCF time-lag computed between 0.3–1 and 3–10 keV; 0.3–10 keV isotropic equivalent peak luminosity in the time interval $t_{\rm i}$–$t_{\rm f}$ as determined from the Norris et al. (2005) profile fit (see Table A1); short-lived (SL) or long-lived (LL) X-ray afterglow according to the classification by Sakamoto & Gehrels (2009).

GRB	z	T_{90} (s)	Γ_γ	EE (s)	$R_{\rm int}$	$t_{\rm i}$ (s)	$t_{\rm f}$ (s)	$\Delta t_{\rm reb}$ (s)	$\tau^x_{\rm lag}$ (s)	$L^{\rm SGRB}_{\rm pk,F}$ (10^{47} erg s^{-1})	X-ray afterglow
050724*	0.258	3.00	1.71 ± 0.16	104.4	0.0117	213.8	340.4	3.00	6.4 ± 2.7	1.49 ± 0.34	LL
051210	–	1.30	1.10 ± 0.30	0	0.0139	87.3	171.0	10.0	5.5 ± 1.9	–	SL
051227	–	8.00	1.31 ± 0.22	119.1	0.0540	101.2	177.2	4.00	-4.5 ± 7.2	–	LL
060313	–	0.74	0.71 ± 0.07	0	0.0005	110.6	250.00	8.00	30.5 ± 25.4	–	LL
070724A	0.457	0.40	1.81 ± 0.33	0	0.0074	73.0	126.0	4.00	3.6 ± 4.6	5.68 ± 2.32	LL
071227	0.383	1.80	0.99 ± 0.22	106.6	0.0356	126.18	201.0	3.00	1.6 ± 1.6	1.13 ± 0.44	LL
090607	–	2.30	1.25 ± 0.30	0	0.0016	76.1	173.3	10.0	3.6 ± 10.4	–	SL
100117A*	0.920	0.30	0.88 ± 0.22	0	0.0030	86.1	238.5	5.00	3.3 ± 1.6	14.09 ± 5.60	SL

requirement above (Table 1).[3] Notably, the sample includes the unique two SGRBs with secure early-type host identification: GRB 050724 (Barthelmy et al. 2005b) and GRB 100117A (Fong et al. 2011). In three cases (GRB 050724, GRB 070724 and GRB 071227, in boldface in Table 1) an extended emission (EE) has been detected in the soft γ-ray energy range after the short hard spike (Norris et al. 2010a; Norris, Gehrels & Scargle 2011). In the other cases, an upper limit on the EE to initial pulse complex (IPC) intensity ratio ($R_{\rm int} \equiv {\rm EE_{int}/IPC_{int}}$) has been provided by Norris et al. (2010a): for the sample of events without EE the upper limit on $R_{\rm int}$ is found to be a factor of $\gtrsim 10$ below the typical $R_{\rm int}$ of SGRBs with detected EE (Table 1, column 7). Finally, GRB 100816A has not been included in the sample in spite of its $T_{90} = 2.9 \pm 0.6$ s (Markwardt et al. 2010) since the low statistics prevents the γ-ray lag analysis from giving definitive results on its possible short nature (Norris et al. 2010b). The burst is however considered a SGRB in Norris et al. (2011).

2.1 *Swift*-BAT data analysis

BAT data have been processed using standard *Swift*-BAT analysis tools within HEASOFT (v. 6.10). In particular, the BATGRBPRODUCT script has been used to generate event lists and quality maps necessary to construct 4 ms mask-weighted and background-subtracted light curves in the 50–100 and 100–200 keV energy bands. The ground-refined coordinates provided by the BAT-refined circulars have been adopted; standard filtering and screening criteria have been applied.

2.2 *Swift*-XRT data analysis

XRT data have been processed with the latest HEASOFT release available at the time of writing (v. 6.10) and corresponding calibration files: standard filtering and screening criteria have been applied. Pile-up corrections have been applied when necessary (Romano et al. 2006; Vaughan et al. 2006). Count-rate light curves have been extracted in the total XRT 0.3–10 keV energy band as well as in the 0.3–1, 3–10, 0.3–1.5, 1.5–10 and 4–10 keV energy bands. The 0.3–10 keV count-rate light curves have been rebinned at a minimum signal-to-noise (S/N) ratio = 4 and then searched for statistically significant temporal variability superimposed over a smooth afterglow decay. A two-step procedure has been followed: first the smooth continuum contribution has been determined applying the method by Margutti et al. (2011). A simple power-law or a smoothly joined broken power-law model is adopted (black solid line of Fig. 1). As a second step, the properties of statistically significant fluctuations with respect to the continuum have been determined adding a number of Norris et al. (2005) profiles to the best-fitting continuum model. The best-fitting Norris et al. (2005) profiles constitute the sample of X-ray flare candidates of SGRBs analysed in this work. Fig. 1 shows GRB 100117A as an example: three distinct episodes of variability have been identified. The best-fitting parameters of the entire sample are listed in Table A1. The choice of the Norris et al. (2005) profile allows us to perform a one-to-one comparison with the properties of X-ray flares and prompt pulses in LGRBs (Chincarini et al. 2010; Bernardini et al. 2011): Fig. 2 shows the evolution of the SGRB flare candidates width with time compared to LGRB flares.

The evolution of the spectral properties of any source can be constrained through the analysis of its HR, which is here defined as HR = counts(1.5–10 keV)/counts(0.3–1.5 keV). A different binning with respect to the total 0.3–10 keV light curve has been used for the 1.5–10 and 0.3–1.5 keV light curves to improve the HR S/N ratio. The temporal evolution of the spectral photon index Γ has been calculated by Evans et al. (2010). Results are portrayed in Figs 1, B1, B2, B3 and B4.

Count-rate light curves have been converted into flux and luminosity (when possible) curves using the spectral information derived from a time-resolved spectral analysis where the spectral evolution of the source, if present, is properly accounted for. This procedure allows us to convert the best-fitting peak count rates of the X-ray flare candidates (A parameter of Table A1) into 0.3–10 keV peak luminosities $L^{\rm SGRB}_{\rm pk,F}$ when the redshift of the source is known. Fig. 3 shows the evolution of the SGRB flare candidate $L^{\rm SGRB}_{\rm pk,F}$ with time compared to the results obtained for LGRB flares by Chincarini et al. (2010); a comparison of the two distributions

[3] The percentage of SGRBs with variable XRT light curve 8/60 $\sim$ 13 per cent is much less than the $\sim$30 per cent of LGRBs showing flares (Chincarini et al. 2010). This result suggests that the percentage of SGRB light curves with variability superimposed is lower than in LGRBs. However, the lower statistics characterizing the SGRB curves prevents us from drawing firm conclusions. This topic will be addressed in a separate work.

Downloaded from http://mnras.oxfordjournals.org/ at NASA Goddard Space Flight Ctr on July 11, 2014

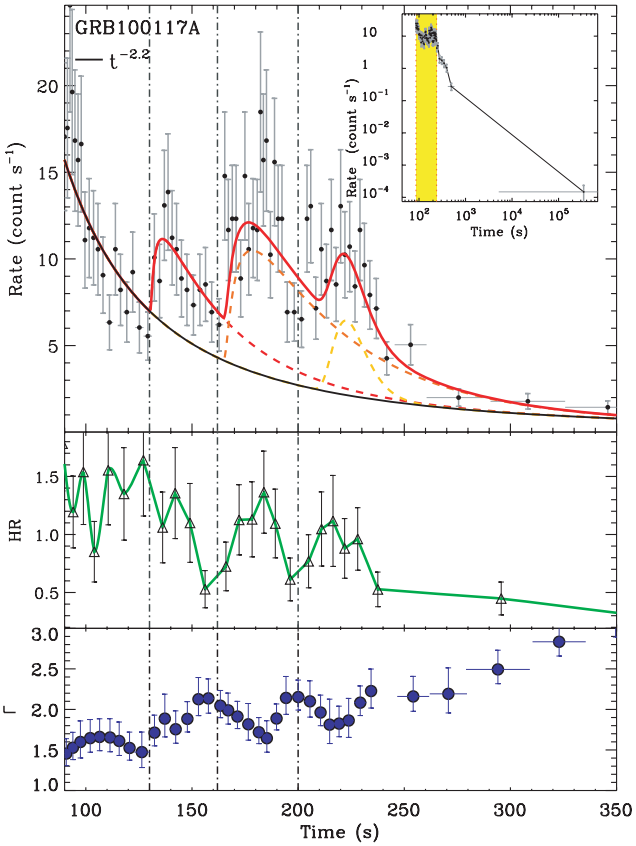

Figure 1. Upper panel: 0.3–10 keV count-rate light curve of GRB 100117A. Black solid line: continuous X-ray emission underlying the flare candidates computed as described in Section 2.2; dashed lines: best-fitting flare candidate emission; red solid line: best estimate of the total emission. The vertical dot–dashed lines mark the flare candidate onset times. Inset: complete *Swift*-XRT light curve. The yellow filled area marks the time window for the computation of the CCF lag (Section 2.3). Middle panel: HR evolution with time; the HR is computed between 1.5–10 (hard band) and 0.3–1.5 keV (soft band). Lower panel: spectral photon index evolution with time as calculated by Evans et al. (2010).

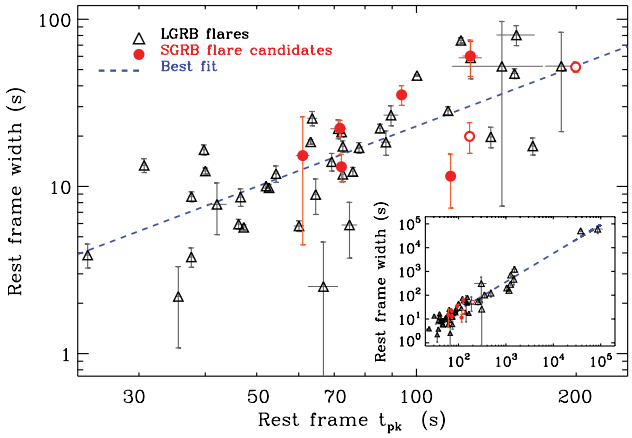

Figure 2. Rest-frame width versus peak time relation for LGRB early-time flares from Chincarini et al. (2010) (open triangles) and SGRB flare candidates with and without extended emission (red open and filled circles, respectively). Inset: complete view of the $w/(1+z)$ versus $t_{\rm pk}/(1+z)$ relation established by LGRB flares obtained joining the data from Chincarini et al. (2010) and Bernardini et al. (2011). The blue dashed line in both plots marks the best-fitting relation calculated on LGRB flares: $[w/(1+z)] = 10^{(-1.0\pm0.5)}[t_{\rm pk}/(1+z)]^{(1.2\pm0.2)}$, where w and $t_{\rm pk}$ are measured in seconds.

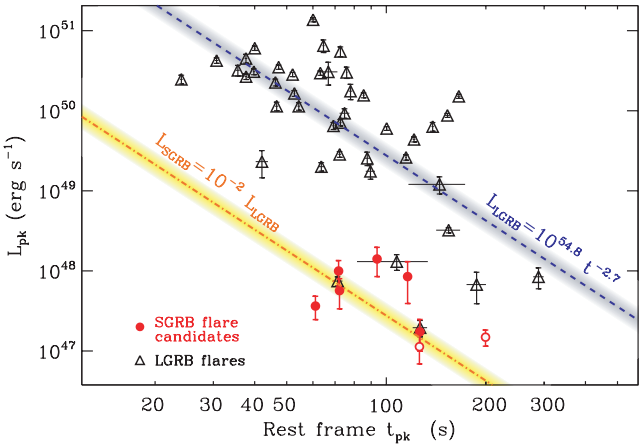

Figure 3. 0.3–10 keV peak luminosity evolution with time for LGRB flares (black open triangles, from Chincarini et al. 2010) and SGRB flare candidates with and without extended emission (red open and filled circles, respectively). Blue dashed line: best-fitting power-law model for LGRB flares: $L_{\rm pk,F}^{\rm LGRB} = 10^{54.8\pm0.4}[t_{\rm pk}/(1+z)]^{-2.7\pm0.5}$ and extrinsic scatter $\sigma = 0.73\pm0.08$. Orange dot–dashed line: best-fitting $L_{\rm pk,F}^{\rm LGRB}$ decay renormalized by a factor of 100 to match the observed SGRB flare candidates $L_{\rm pk,F}^{\rm SGRB}$.

can be found in Fig. 4. The isotropic equivalent energy $E_{\rm iso,F}^{\rm SGRB}$ has been determined integrating the best-fitting Norris et al. (2005) luminosity-calibrated profiles from the onset time ($t_{\rm s}$) to $t_{\rm s} + 100w$ (where w is the flare candidate width). The uncertainty arising from the spectral calibration has been propagated following standard practice into the final $L_{\rm pk,F}^{\rm SGRB}$ and $E_{\rm iso,F}^{\rm SGRB}$ uncertainties listed in Tables 1 and A1. We refer the reader to Margutti et al. (2010a) for details on the light curves and spectra extraction. Fig. 5 shows the SGRB flare candidates $E_{\rm iso,F}^{\rm SGRB}$ distribution compared to the values determined for LGRB flares, as computed by Chincarini et al. (2010).

2.3 Spectral time-lag computation

The spectral lag is the time difference between the arrival of high-energy and low-energy photons. For each GRB, the X-ray and γ-ray spectral lags ($\tau_{\rm lag}^{x}$ and $\tau_{\rm lag}^{\gamma}$, respectively) and associated uncertainties have been determined using a cross-correlation function (CCF) analysis. The CCF analysis requires the observations to have a fractional exposure equal to 1: this requirement excludes most of XRT observations taken in photon counting (PC) mode.[4] Among these, the late-time ($t \sim 5\times10^4$ s) rebrightening of GRB 050724 (Fig. B1). We closely follow the prescriptions by Stamatikos et al. (2009) and Ukwatta et al. (2010) for the CCF computation: in particular, each CCF peak has been fitted using a third order polynomial; the

[4] *Swift*-XRT automatically switches to the PC observing mode for count-rates below a few count s^{-1} to minimize the presence of pile-up. In PC mode, it is not uncommon to have short time intervals of no observation even during a single orbit. While the light curve and spectra extraction procedures are basically insensitive to these short pauses, the CCF analysis would give unreliable results.

© 2011 The Authors, MNRAS **417,** 2144–2160
Monthly Notices of the Royal Astronomical Society © 2011 RAS

Downloaded from http://mnras.oxfordjournals.org/ at NASA Goddard Space Flight Ctr on July 11, 2014

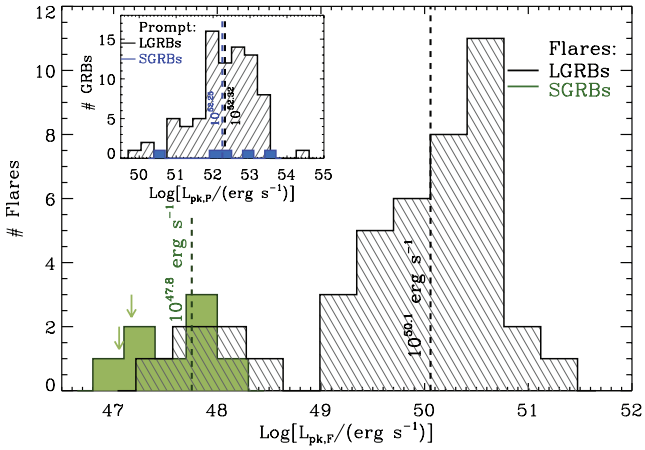

Figure 4. 0.3–10 keV (observer frame) isotropic equivalent peak luminosity $L_{\rm pk,F}^{\rm LGRB}$ of LGRB flares from Chincarini et al. (2010) (hatched histogram) compared to SGRB flare candidates (filled histogram); two vertical arrows mark the position of flare candidates in SGRBs with extended emission. The vertical dashed lines mark the median values of the two distributions: $L_{\rm pk,F}^{\rm LGRB} \sim 10^{50.1}$ erg s^{-1}; $L_{\rm pk,F}^{\rm SGRB} \sim 10^{47.8}$ erg s^{-1}. Inset: 1–10 000 keV rest-frame isotropic equivalent peak luminosity distribution of the LGRBs (Nava et al. 2008) and SGRBs prompt emission (Ghirlanda et al. 2009; Ghirlanda 2010), with median value: $L_{\rm pk,P} \sim 10^{52.3}$ erg s^{-1}.

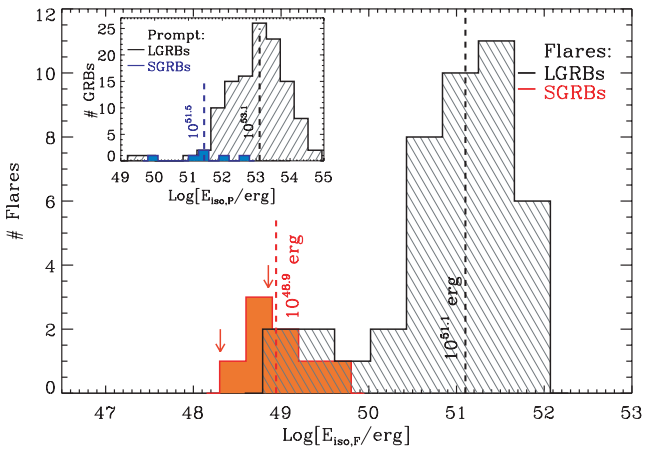

Figure 5. 0.3–10 keV (observer frame) isotropic equivalent energy $E_{\rm iso,F}^{\rm LGRB}$ of LGRB flares from Chincarini et al. (2010) (hatched histogram) compared to SGRB flare candidates (filled histogram); two vertical arrows mark the position of flare candidates in SGRBs with extended emission. Vertical dashed lines: median $E_{\rm iso,F}^{\rm LGRB} \sim 10^{51}$ erg and $E_{\rm iso,F}^{\rm SGRB} \sim 10^{49}$ erg values. Inset: 1–10 000 keV rest-frame isotropic equivalent energy distribution for the prompt emission of the widest samples of LGRBs (hatched histogram) and SGRBs (filled histogram) with firm spectral parameter estimates at the time of writing (Amati et al., in preparation), with median values: $E_{\rm iso,P}^{\rm LGRB} \sim 10^{53.1}$ erg; $E_{\rm iso,P}^{\rm SGRB} \sim 10^{51.5}$ erg.

number of points to be fitted around the CCF peak has been allowed to vary from case to case with the possibility to specify asymmetric intervals around the peak. In our analysis, a positive spectral lag is obtained if high-energy photons lead low-energy photons.

The lag extraction is sensitive to a number of parameters: energy band pass of each comparative light curve, temporal bin resolution, S/N ratio and presence of background emission (i.e. in X-rays, the smooth X-ray decay underlying the time-variable signal). For the prompt γ-ray phase, the lag has been calculated using 4 ms light curves (Section 2.1) in the 50–100 and 100–200 keV energy bands. Time intervals covered by extended emission have been excluded. This allows us to perform a direct comparison with the time-lag values obtained for LGRBs observed by BAT (Ukwatta et al. 2010). Results are listed in Table 1, column 5: the eight SGRBs exhibit negligible $\tau_{\rm lag}^{\gamma}$.

In the X-rays the situation is complicated by the presence of a smoothly declining afterglow emission underlying the episodes of possible activity (see e.g. black solid line of Fig. 1). Choices of re-binning time-scales, energy bands and/or temporal intervals giving origin to correlation values (CCF peak) <0.4 have been discarded. The choice of the energy bands to be compared is limited by the XRT 0.3–10 keV coverage. For each SGRB, the X-ray time lag $\tau_{\rm lag}^{x}$ has been computed for different energy bands, giving consistent results: the 0.3–1 and 3–10 keV energy bands have been finally chosen to perform a one-to-one comparison to the results obtained by Margutti et al. (2010b) for flares detected in LGRBs. To this end, the LGRB flare time lags from Margutti et al. (2010b) have been recalculated using the CCF analysis above (black dots in Fig. 6): in Margutti et al. 2010b a *pulse peak* lag was instead calculated (grey dots in Fig. 6). The pulse peak lag is defined as $\tau_{\rm lag}^{\rm peak} \equiv t_{\rm peak}{}^{\rm I} - t_{\rm peak}^{\rm II}$, where $t_{\rm peak}^{\rm I}$ and $t_{\rm peak}^{\rm II}$ are the peak times of the best-fitting profiles in the energy bands I and II, respectively. As such, $\tau_{\rm lag}^{\rm peak}$ is sensitive to the assumed pulse fitting model: while the dependency is limited in cases of bright events, the limited statistics of the SGRB X-ray light curves would cause the pulse *peak* lag computation to be inaccurate. For this reason we refer to the *CCF time-lag* for both short and long GRB data, in the γ-ray and X-ray regimes. The light-curve time binning can potentially affect the derived $\tau_{\rm lag}^{x}$: for each SGRB the lag has been computed on light-curve pairs with 10 different time binnings spanning the range 0.2–20 s. The optimal time binning is defined as the lowest time-scale giving origin to a CCF peak >0.4 and is listed in Table 1. Larger binning time scales have been checked to produce consistent lag results. The window of time of investigation ($t_{\rm i}$ and $t_{\rm f}$ of Table 1) has been determined selecting the time interval containing positive, at least 1σ significant fluctuations around the smooth X-ray continuum (see Margutti et al. 2011 for details).

For each SGRB, $t_{\rm i}$ and $t_{\rm f}$ have been varied of ∼20 per cent both towards larger and lower values: consistent time lag values have been found. The sensitivity of the lag measurement to the smooth X-ray light-curve decay underlying the candidate flares has been investigated calculating the lag $\tau_{\rm lag}^{x,\rm sub}$ on light-curve pairs where the contribution of the smooth afterglow component has been properly subtracted and uncertainties propagated following the prescriptions by Margutti et al. (2011). For each SGRB this procedure has led to consistent $\tau_{\rm lag}^{x,\rm sub} - \tau_{\rm lag}{}^{x}$ values ($\tau_{\rm lag}^{x,\rm sub}$ systematically has larger uncertainties due to the lower S/N ratio of the subtracted light curves). For this reason we refer to $\tau_{\rm lag}^{x}$ hereafter. Finally, we have tested and verified the robustness of our choice of energy bands to be compared, rebinning times and window of time of investigation, by performing a number of simulations where artificial lags have been first introduced into the light curves and then successfully recovered. Results are reported in Table 1. Fig. 6 combines the $\tau_{\rm lag}^{x}$ and $L_{\rm pk}$ luminosity information in the lag–luminosity plane and clearly shows that SGRB flare candidates fall off the prediction based on LGRB flares and prompt pulses.

3 RESULTS

The data analysis of the previous sections leads to the following results.

Downloaded from http://mnras.oxfordjournals.org/ at NASA Goddard Space Flight Ctr on July 11, 2014

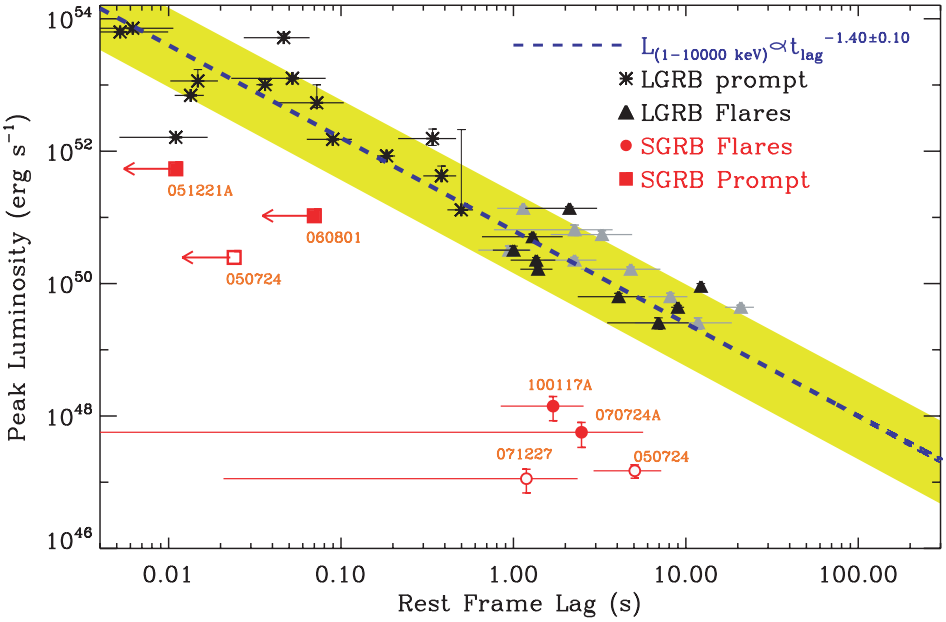

Figure 6. Lag–luminosity plot. Red circles: CCF lag for candidate flares of SGRBs: open symbols refer to SGRBs with detected EE; black (grey) triangles: CCF (pulse peak) lag for the sample of nine flares of LGRBs of Margutti et al. (2010b), their fig. 15. Black stars: prompt γ-ray data from the gold and silver sample of Ukwatta et al. (2010). Red squares: 3σ upper limits to the prompt lag of SGRBs for which it is possible to estimate the peak luminosity: open symbols refer to SGRBs with detected EE. The isotropic peak luminosity is computed in the 1–10^4 and 0.3–10 keV bands for prompt data and X-ray flares, respectively; the lag corresponds to the time difference between light-curve structures in the 50–100 and 100–200 keV channels (prompt data) and 0.3–1 and 3–10 keV channels (X-ray flares). Blue dashed line: best-fitting law for the LGRB *prompt* emission data.

(i) SGRB flare candidates appear both in early-type and late-type host galaxy environments, irrespective of the short-lived (SL) or long-lived (LL) nature of the X-ray afterglow.

(ii) Both SGRBs with a bright EE and SGRBs which lack this component show cases of statistically significant fluctuations superimposed over smoothly decaying X-ray light curves (Table 1).

(iii) Flares in LGRBs are known to show a spectral hardening during the rise time and a softening during the decay time, reminiscent of the prompt emission (e.g. Margutti et al. 2010b and references therein): as a result the HR evolution mimics the flare profile (see e.g. Goad et al. 2007, their fig. 9) while the spectral photon index evolution anticorrelates with the flare flux. In spite of the lower statistics and limited $\Delta F/F$ of SGRB flare candidates (Fig. 7), we find in the case with the best statistics a hint for correlation between the HR evolution and the temporal profile of GRB 101117A, with a photon index evolution that anticorrelates with the flux of the flare candidates (Fig. 1, middle and lower panels). In the other cases (Figs B1–B4) the limited statistics prevents us from drawing firm conclusions.

(iv) The SGRB flare candidates width evolution is roughly linear in time and consistent with the $w/(1+z)$ versus $t_{\rm pk}/(1+z)$ relation established by LGRB flares over ~four decades in time (Fig. 2). The best-fitting law reads: $w/(1+z) = 10^{-1.0\ \pm0.5}[t_{\rm pk}/(1+z)]^{1.2\ \pm0.2}$. It is remarkable that data coming from LGRB flares both at early and very late time (beyond $t_{\rm pk}/(1+z) \sim 10^5$ s, Fig. 2, inset) as well as temporal fluctuations in completely different systems like SGRB afterglows are consistent at zero-order with the same, approximately linear, law. We refer to Bernardini et al. (2011) for a discussion of the possible bias affecting the w versus $t_{\rm pk}$ relation.

(v) SGRB flare candidates are ~100 times dimmer than LGRB flares at the same rest frame time (Fig. 3). Selecting the sub-sample of LGRB flares detected in the same rest frame time interval 60 s $\lesssim t_{\rm pk}/(1+z) \lesssim$ 250 s of SGRB flare candidates, we obtain a median $\langle L^{\rm LGRB}_{\rm pk,F}\rangle \sim 10^{49.8}$ erg s^{-1} to be compared to $\langle L^{\rm SGRB}_{\rm pk,F}\rangle \sim 10^{47.8}$ erg s^{-1} of the SGRB sample showed in Fig. 4. As a result, SGRB flare candidates fall off of a factor of ~100 the peak luminosity versus time relation established by LGRB flares which reads: $L^{\rm LGRB}_{\rm pk,F} = 10^{54.8\ \pm0.4}[t_{\rm pk}/(1+z)]^{-2.7\ \pm0.5}$.

(vi) Short and long GRBs show a comparable 1–10^4 keV (rest frame) isotropic peak luminosity during their prompt emission, with a median $\langle L_{\rm pk,P}\rangle \sim 10^{52.3}$ erg s^{-1} (Fig. 4, inset). On the contrary, the peak luminosity of flares of both categories evaluated at the same rest frame time $60 < t_{\rm pk}/(1+z) < 200$ s differ of a factor of ~100 as noted above. While for LGRBs the typical prompt (1–10^4 keV) to flare (0.3–10 keV) peak luminosity ratio $(L^{\rm LGRB}_{\rm pk,P}/L^{\rm LGRB}{}_{\rm pk,F}) \sim 300$, for SGRBs the same quantity reads: $(L^{\rm SGRB}_{\rm pk,P}/L^{\rm SGRB}{}_{\rm pk,F}) \sim 3 \times 10^4$. Flare candidates in SGRBs are therefore *less luminous* than expected using the prompt-to-flare luminosity scaling observed in LGRBs at the same flare rest frame time.[5]

(vii) SGRB flare candidates are ~100 times *less energetic* than LGRB flares (Fig. 5), with a median 0.3–10 keV energy $\langle E^{\rm SGRB}_{\rm iso,F}\rangle \sim 10^{48.9}$ erg ($\langle E^{\rm LGRB}_{\rm iso,F}\rangle \sim 10^{50.9}$ erg). Since the width of LGRB flares and SGRB flare candidates are comparable when evaluated at the same $t_{\rm pk}/(1+z)$, this result is a natural consequence of the $\langle L^{\rm LGRB}_{\rm pk,F}\rangle/\langle L_{\rm pk,F}{}^{\rm SGRB}\rangle \sim 100$ reported above. On average, in the time interval 60 $\lesssim t_{\rm pk}/(1+z) \lesssim$ 250 s a flare in a LGRB emits ~0.6 per cent of the 1–10^4 keV prompt $E^{\rm LGRB}_{\rm iso,P}$; the observed SGRB flare

[5] The prompt emission peak luminosity is likely to be biased towards the bright end of the real $L_{\rm pk,P}$ distribution, since a minimum S/N ratio is needed to constrain the spectral parameters and calculate $L_{\rm pk,P}$ in the 1–10^4 keV range: this requirement is more severe in the case of SGRBs whose observed emission is usually less bright than LGRBs. However, Fig. 8 shows that the main conclusion of this paragraph remains true even after relaxing the requirement above.

Downloaded from http://mnras.oxfordjournals.org/ at NASA Goddard Space Flight Ctr on July 11, 2014

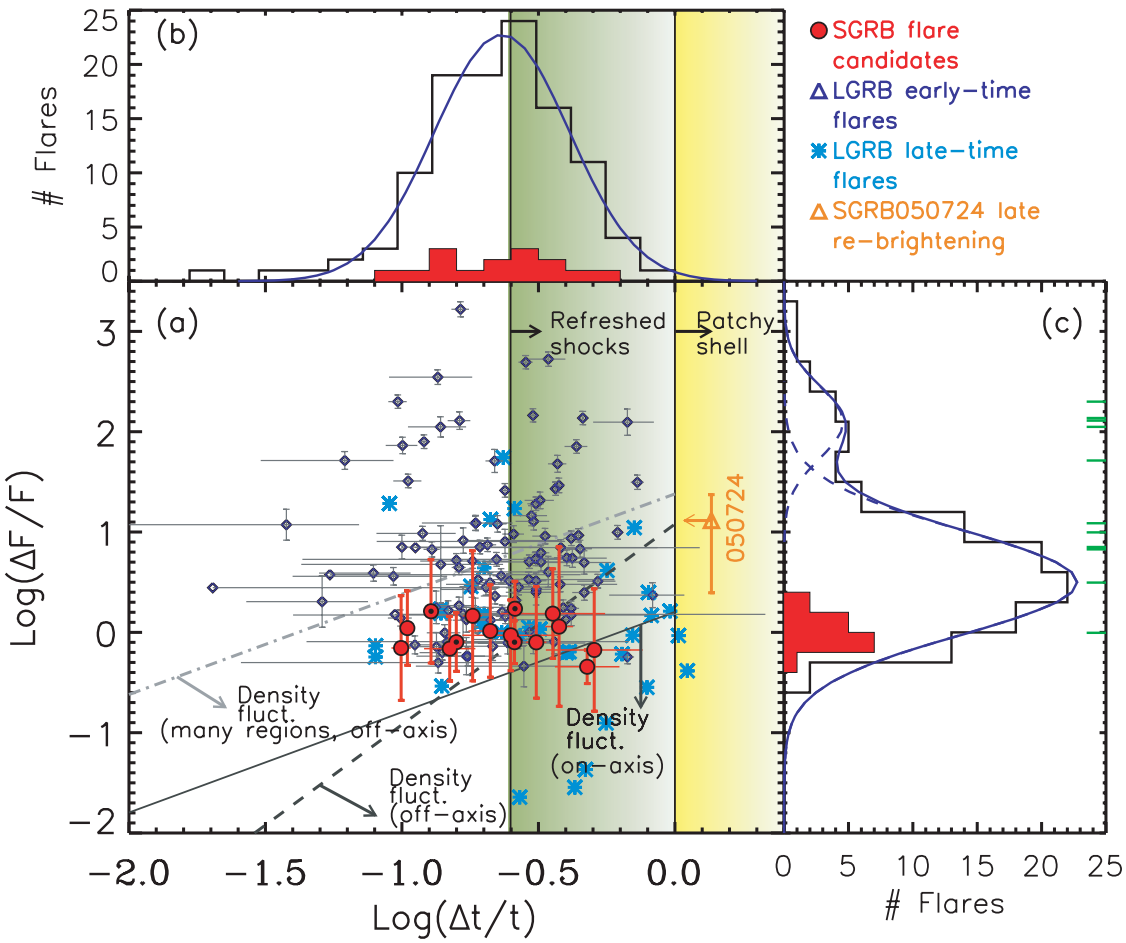

Figure 7. Panel (a): relative variability flux $\Delta F/F$ versus relative variability time-scale $\Delta t/t \equiv w/t_{\rm pk}$ for the sample of X-ray flare candidates in SGRBs (filled circles), compared to early- and late-time LGRB X-ray flares (blue open diamonds and light-blue stars, respectively) from Chincarini et al. (2010) and Bernardini et al. (2011). The late-time rebrightening detected in GRB 050724 is also shown for completeness with an orange open triangle (Bernardini et al. 2011). A small black dot marks data coming from SGRBs with detected extended emission. Solid, dashed and dot–dashed lines mark the kinematically allowed regions in different scenarios according to Ioka et al. (2005), their equations (7) and (A2). The $\Delta t/t$ and $\Delta F/F$ distributions are portrayed in panels (b) and (c) adopting the same colour coding. The green tick marks in panel (c) show the flux contrast for the subsample of LGRB flares of Fig. 6.

candidates isotropic energy is ∼0.2 per cent the 1–10^4 keV prompt $E_{\rm iso,P}^{\rm SGRB}$.[6]

(viii) Flares and prompt pulses in LGRBs define a spectral lag-peak luminosity relation (Fig. 6): this finding is highly suggestive of a common origin (Margutti et al. 2010b).[7] On the contrary, SGRB prompt pulses are known to exhibit much shorter lags than expected if they were to follow the LGRB prompt pulses lag–luminosity relation (e.g. Gehrels et al. 2006). Fig. 6 extends this behaviour to their flare candidates: like SGRB prompt pulses, flare candidates in SGRBs *fall off* the lag–luminosity relation defined by LGRBs.

(ix) Flares candidates of SGRBs in the $\Delta F/F$ versus relative variability time-scale ($\Delta t/t \equiv w/t_{\rm pk}$) plane are compatible with variability arising from density fluctuations of many regions viewed off-axis: on the contrary, neither the refreshed-shock nor the patchy-shell scenario is able to account for the observed properties of the entire sample (see Ioka et al. 2005 for details on the definition of the various scenarios).[8] In particular: a K–S test comparing the $\Delta t/t$ distributions of LGRB flares and SGRB flare candidates reveals that they belong to the *same* parent population at ∼10 per cent level of probability; the probability reaches the 88 per cent level if LGRB flares are selected in the SGRB peak time range ($60 \lesssim t_{\rm pk}/(1+z) \lesssim 250$ s). This is consistent with the common $w/(1+z)$ versus $t_{\rm pk}/(1+z)$ relation followed by short and long GRBs discussed above. On the contrary, no X-ray flare candidate in a SGRB shows a relative variability flux $\Delta F/F > 2$ in strong *contrast* with the LGRB $\Delta F/F$ distribution at comparable $t_{\rm pk}/(1+z)$ (Fig. 7). Such prominent flares would be easier to detect, so that it is unlikely that

[6] Again, this ratio is likely to be a lower limit to real value due to the bias affecting the sample of SGRBs with prompt $E_{\rm iso}$ measure discussed in the previous paragraph.

[7] Note that flare and prompt lags are calculated in different energy bands and are not directly comparable. The fact that flares define a lag–luminosity relation with slope very similar to the prompt data is however suggestive of a strict connection between flares and prompt pulses. See Margutti et al. (2010b) for details.

[8] The smoking gun against a refreshed shock scenario would be the detection of a spectral change contemporaneous to the flare candidates: while the statistics of the XRT light curves of SGRBs is limited, in the case with best statistics the HR evolution is correlated to the candidate flare profiles and the continuum after the flaring emission is softer than the emission detected during the period of temporal variability (Fig. 1). These findings favour an alternative explanation.

Downloaded from http://mnras.oxfordjournals.org/ at NASA Goddard Space Flight Ctr on July 11, 2014

Table 2. Summary of the properties of SGRB flare candidates compared to LGRB X-ray flares observed at the *same* $t_{\rm pk}/(1+z)$.

Property	=	≠
Width	$w(t_{\rm pk})$	
Relative variability	$\Delta t/t$	
Relative variability flux		$\Delta F/F$
Peak luminosity		$\frac{L^{\rm SGRB}_{\rm pk,F}}{L^{\rm LGRB}_{\rm pk,F}} \sim 0.01$
Isotropic energy		$\frac{E^{\rm SGRB}_{\rm iso,F}}{E^{\rm LGRB}_{\rm iso,F}} \sim 0.01$
Lag–luminosity		$L_{\rm pk}(\tau^{x}_{\rm lag})$
Flare to prompt energy ratio	$E_{\rm iso,F}/E_{\rm iso,P}$	
Flare to prompt luminosity ratio		$L_{\rm pk,F}/L_{\rm pk,P}$
Flare to prompt pulse width ratio		$w_{\rm F}/w_{\rm P}$

an observational bias could explain the present lack of detection. A K–S test comparing the two distributions shows that the probability that LGRB and SGRB flare candidates share the same $\Delta F/F$ parent population is as low as 3.3×10^{-4}. This result partially inherits the uncertainty affecting the completeness of both distributions for very small $\Delta F/F$ values. Another source of uncertainty arises from the difficulty in evaluating the continuum underlying the possible flare emission in SGRBs when data are particularly sparse. In spite of these limitations, after more than 6 years of *Swift* observations (and ∼60 SGRB afterglows detected) there is still no SGRB showing a prominent ($\Delta F/F > 10$) fast-variability $\Delta t/t \ll 1$ feature during its X-ray afterglow. The SGRB flare candidate $\Delta F/F$ is instead more similar to the relative variability flux of flares in LGRBs detected at *late* times ($t_{\rm pk} > 1$ ks, light-blue stars in Fig. 6, main panel; Bernardini et al. 2011): the two $\Delta F/F$ distributions share the same parent distribution at ∼21 per cent level of probability (K–S test).

The results above demonstrate the complexity characterizing the SGRB flare candidates phenomenology: Table 2 reports a summary of their properties when compared to LGRB flares. The main result is that the population of SGRB X-ray flare candidates only *partially* share the set of observational properties of LGRB X-ray flares detected at the same rest frame time: are there real X-ray flares in SGRBs? A detailed discussion is provided below.

4 DISCUSSION

Observations show that like LGRBs, at least some SGRB X-ray afterglows deviate from a smooth power-law decay and show variability. In the following we discuss the properties of SGRB flare candidates providing a one-to-one comparison with LGRB X-ray flares. The aim is to better understand the origin of the short burst afterglow variability and uncover potential links with the prompt phase.

With $\Delta t/t > 1$, the late-time ($t_{\rm pk} \sim 5 \times 10^4$ s) rebrightening of GRB 050724 strongly differs from the properties of the entire sample of flare candidates detected in SGRBs thus questioning its classification as flare-like episode (Panaitescu 2006; see however Campana et al. 2006; Grupe et al. 2006; Malesani et al. 2007). Malesani et al. (2007) report the detection of an optical and radio rebrightening associated to the X-ray bump which is unusual if compared to the standard properties of X-ray flares, while being more common to late-time rebrightenings observed in LGRBs as well (see e.g. GRB 081028; Margutti et al. 2010a). In addition, no hard-to-soft evolution can be detected in the X-ray data (Evans et al. 2010), which is instead typical of flares (Goad et al. 2007) and prompt pulses in LGRBs (Hakkila & Preece 2011). In the following we focus our attention on SGRBs fast variability ($\Delta t/t < 1$) referring the reader to Bernardini et al. (2011) for a complete discussion of the late-time behaviour of GRB 050724.

4.1 SGRB local and global environment

The standard model (see Nakar 2007 for a recent review) explains the X-ray afterglow of long and short GRBs as synchrotron radiation arising from the deceleration of a relativistic blast wave into the external medium. If the shock front is homogeneous and expands into a smooth ambient density, a smooth afterglow light curve is expected. In this context, variability in the X-ray afterglow could be caused by re-freshed shocks (i.e. shocks caused by slow shells catching up with the leading, decelerated shell at late times, Kumar & Piran 2000a, Granot, Nakar & Piran 2003): Fig. 7 shows that half of the SGRB flare candidates sample do not comply with this scenario.[9] Furthermore, the spectral variability shown in Fig. 1, lower panel, makes it difficult to interpret the flare candidates in the re-freshed shocks scenario.

A first alternative is to relax the assumption on the homogeneity of the shock front (Kumar & Piran 2000b): an intrinsic angular structure of the emitting surface is able to produce variability with a characteristic time-scale $\Delta t \geq t$ if the angular fluctuation is persistent (patchy shell model, Nakar & Oren 2004):[10] no SGRB flare candidate is consistent with this expectation (Fig. 7, main panel).

A second alternative invokes the presence of ambient density fluctuations either caused by turbulence in the ISM or by variable winds from the progenitor. From Table 1 it is however apparent that temporal X-ray variability has been detected for SGRBs residing both in early-type and late-type host galaxies which likely have very different ISM properties. In particular GRB 050724 and GRB 100117A are the unique two SGRBs with secure early-type host galaxy association (Barthelmy et al. 2005b; Fong et al. 2011). This suggests that the ISM turbulence is unlikely to provide a feasible physical mechanism for the detected variability. Note however that the limited size of our sample prevents us from quantitatively discussing the correlation between the appearance of flare candidates and host environment.

Different progenitor models of SGRBs lead to distinct predictions on their *local* environment as well. In particular, according to the standard compact binary merger scenario (NS–NS or NS–BH; Eichler et al. 1989; Narayan et al. 1992), no variable wind is expected from the progenitor. An origin of SGRB flare candidates from density fluctuations of the circumburst environment is therefore considered unlikely. Alternative scenarios leading to SGRB environments with circumburst densities comparable to LGRBs have been however explored by Nysewander et al. (2009) to explain the similar F_R/F_X ratio (where F_R and F_X stand for the afterglow flux density at 11 h post-trigger in the R- and X-ray bands, respectively). A systematic difference between sub-galactic environments able or unable to produce variability in the X-ray afterglow could in principle be revealed by different offsets with respect to the host galaxy centres: however, the present sample of SGRBs with flare candidates includes both SGRB with large offsets (e.g.

[9] See however Granot et al. (2003) and Vlasis et al. (2011): sharp *optical* and *radio* flares could be produced by collision of ultrarelativistic shells.
[10] Details on variability arising from a time-varying anisotropic emitting surface can be found in Ioka et al. (2005).

© 2011 The Authors, MNRAS **417,** 2144–2160
Monthly Notices of the Royal Astronomical Society © 2011 RAS

Downloaded from http://mnras.oxfordjournals.org/ at NASA Goddard Space Flight Ctr on July 11, 2014

$\delta = 14.80 \pm 0.34$ kpc for SGRB 071227; D'Avanzo et al. 2009; Fong, Berger & Fox 2010) and events with very small offsets (e.g. $\delta = 0.47 \pm 0.31$ kpc, SGRB 100117A; Fong et al. 2011). While the observed offset distribution is incomplete, these data suggest that the properties of the *local* environment of SGRBs are not the key parameters determining the presence of flare candidates in their X-ray light curves. This conclusion is strengthened by the results of Section 4.5.

Flares candidates and prompt pulses could alternatively share a common origin. *In this case, flare candidates would bring no information on the external medium density. We refer to this interpretation as the '*internal origin*' possibility (see Section 4.7).

4.2 Flare candidates and extended emission

Three bursts in our sample (boldface in Table 1) present evidence for EE: a long-lasting ($\Delta t \sim 10^2$ s) soft X-ray tail that follows the short hard spike in the prompt phase. Norris et al. (2010a) analysed a sample of 51 *Swift*-BAT SGRBs looking for the presence of EE in their γ-ray data and concluded that ~3/4 of the BAT SGRBs are *not* accompanied by an EE component. In particular, in this work it is shown that the *upper limit* on the EE to IPC (initial pulse complex) intensity ratio of the SGRBs of our sample (i.e. with flare candidates) not showing EE is a factor $\gtrsim$10 below the standard values found for GRBs with EE (Norris et al. 2010a, their fig. 1). This implies that in those cases the EE is either very weak or absent. The inverse is also true: some SGRBs with bright EE are accompanied by a smooth X-ray light curve at $t \gtrsim 80$ s (see e.g. GRB 080503, Norris et al. 2010a, their table 1).

While it is still unclear if the origin of the EE component is related to the prompt emission, the afterglow or a third, unknown physical process (Perley et al. 2009; Norris et al. 2010a; Norris et al. 2011), our analysis shows that the presence of a bright EE does not imply the presence of flare candidates and vice versa. We stress that the higher average brightness characterizing the XRT light curves of GRBs with EE with respect to those without EE, would naturally bias the result in the opposite direction (i.e. it would favour temporal fluctuations to be detected in XRT light curves with the best statistics, leading to a biased flare–EE connection) thus strengthening our conclusion. The limited size of our sample (which is however the widest possible at the time of writing) does not allow us to quantitatively discuss the flare candidates versus EE correlation (or lack thereof).

Our analysis cannot however exclude that SGRB flare candidates constitute temporal fluctuations superimposed on (and physically linked to) the X-ray tail of the EE, as suggested by the epoch of flare candidates detection ($t_{\rm pk}/(1+z) \lesssim 200$ s). Furthermore, the limited range spanned by the flare-to-continuum flux ratio $\Delta F/F$ (with $\Delta F/F \sim 1$, Fig. 7) is suggestive of a physical link between flare candidates and the underlying continuum (i.e. the EE). Again, flare candidates would be associated to both bright and faint (undetected in the γ-rays) EEs.

4.3 Time-scales

The relative time-scale distribution $\Delta t/t$ of SGRB flare candidates (Fig. 7, upper panel) is compatible with being drawn from the *same* parent population of flares detected in LGRBs at similar $t_{\rm pk}/(1+z)$ at ~88 per cent level of probability: with a median value of $\langle \Delta t/t \rangle = 0.25$ and extending from 0.1 up to 0.5 it furthermore satisfies the limit $\Delta t/t \leq 1$ which is the classical argument against fluctuations arising from the external shock (e.g. Zhang et al. 2006). The $\Delta t/t$ distribution therefore does not support an external shock origin for flare candidates in SGRBs (see however Dermer 2008), in agreement with the findings of Section 4.1.

The evolution of the flare duration with time $w(t_{\rm pk})$ for $t_{\rm pk} > T_{90}$ (Fig. 2) observationally distinguishes flares from prompt pulses in LGRBs (Margutti et al. 2010b): as time proceeds, LGRB flares becomes wider and wider following the best-fitting law: $w/(1+z) \sim (t_{\rm pk}/(1+z))^{1.2\pm0.2}$. This quasi-linear regime establishes for $t_{\rm pk}/(1+z) > T_{90}/(1+z)$, and extends 4 decades in time up to $t_{\rm pk}/(1+z) \gtrsim 10^5$ s. Notably, while the $E_{\rm iso,P}^{\rm LGRB}$ released during the LGRB prompt emission spans more than 3 decades in energy (Fig. 5), likely reflecting different properties of the LGRB central engines, the *duration* of subsequent episodes of activity seems to follow a universal evolution with limited dependence on the initial energy budget. Flares with different amplitudes A, flux ratios $\Delta F/F$ and fluences show similar $w/(1+z)$ when appearing at the same $t_{\rm pk}/(1+z)$ (Chincarini et al. 2010), suggesting that the main parameter driving the flare width evolution in a LGRB is the elapsed time from the explosion $t_{\rm pk}/(1+z)$[11].

Fig. 2 shows that flare candidates in SGRBs are consistent with the *same* quasi-linear temporal scaling: from the width measurement it is not possible to distinguish a flare in a LGRB from a flare candidate in a SGRB. The temporal properties of the prompt emission of LGRBs and SGRBs are clearly different in terms of duration and variability (e.g. Nakar & Piran 2002a): however, ~30 s later, the width of fluctuations superimposed over their X-ray light curves seems to have lost any information on the nature of central engines able to produce γ-ray photons with such different temporal properties. In both cases the w evolution is driven by the $t_{\rm pk}$, irrespective of their different initial conditions (and initial variability time scales): while for flares $w_{\rm F}^{\rm SGRB}/(1+z) \sim w_{\rm F}{}^{\rm LGRB}/(1+z)$ at similar $t_{\rm pk}/(1+z)$, for prompt pulses $w_{\rm P}^{\rm SGRB} \ll w_{\rm P}{}^{\rm LGRB}$ (with $w_{\rm P}^{\rm SGRB} \sim 0.05$ s to be compared to $w_{\rm P}^{\rm LGRB} \sim 1$ s, observer frame values, Nakar & Piran 2002a; Nakar & Piran 2002b).[12]

This finding strongly suggests that the origin of the quasi-linear $w/(1+z)$ versus $t_{\rm pk}/(1+z)$ scaling must be within what is in common for the long and short GRB models, irrespective of the progenitors, environment, lifetime, variability time-scales and prompt energy release of their central engines. Both models require the prompt emission to originate from a relativistic outflow (see e.g. Piran 2004): if the longer and longer duration of flares is of dynamical origin and dominated by the expansion of the emitting regions, no memory of the properties of the central engine which launched the relativistic outflow would be preserved so that long and short GRBs would display flares with similar $w(t_{\rm pk})$. Alternatively, in the context of accretion models the $w(t_{\rm pk})$ relation originates from the viscous evolution of the hyper-accreting disc around the newly born black hole, common ingredient of the likely progenitors of the two classes (Perna et al. 2006). Our results would imply a strict analogy between the mechanisms that regulate the late-time evolution of accreting discs originating from collapsars and mergers of compact objects, irrespective of their different masses and life times (according to the standard scenario accreting discs related to SGRBs are likely to be less massive then LGRB discs and short-lived, as suggested by the observed prompt duration. See Nakar 2007 for details).

[11] As a second level of approximation, one should consider that more prominent flares ($A \gg 1$) tend to be wider (Margutti et al. 2010b).

[12] Note however that the first 1-2 s of bright LGRBs display variability time scales comparable to the SGRB prompt emission, Nakar & Piran (2002a).

Downloaded from http://mnras.oxfordjournals.org/ at NASA Goddard Space Flight Ctr on July 11, 2014

Lazzati et al. (2011) recently suggested that instabilities arising from the propagation of the jet through the disrupting star could explain the presence of flares in LGRBs with $\Delta F/F \lesssim 10$. Even assuming a continuous and featureless release of energy by the central engine, the pressure of the surrounding stellar material would provide the physical origin for the intermittent flare behaviour, naturally explaining the universal (i.e. with limited sensitivity on the star properties and energy budget) quasi-linear $w(t_{\rm pk})$ relation (Lazzati et al. 2011, their equation 6). However this model cannot account either for presence of flares in SGRBs or for their similarity to LGRB flares in the $w/(1+z)$ versus $t_{\rm pk}/(1+z)$ plane: according to the majority of SGRB progenitor scenarios the engine is 'exposed' and there is no stellar material the jet could interact with. As a consequence, if the $w(t_{\rm pk})$ relation in LGRBs originates from the interaction with the progenitor stellar material, it is difficult to explain why flare candidates in SGRBs, while originating from a completely different physical scenario, are however consistent with the same relation, as observed. Our results therefore imply that either the LGRB flare $w(t_{\rm pk})$ relation does not originate from the jet-stellar material interaction or that the progenitors of long and short GRBs are much more similar than previously thought (see e.g. Lazzati, Morsnony & Begelman 2010).

Finally, our findings suggest that while the variability time scales measured during the prompt emission could still directly reflect the intrinsic variability of the central engine (see Piran 2004 and references therein), absolute measures (i.e. not renormalized) of flare widths likely do not (if time-dilated by physical mechanisms which are only indirectly related to the central engine). On the contrary, the *ratio* of interesting time-scales of the same flare profile, being subject to the same temporal stretching, could still retain an imprint of the original mechanism at work: this would explain why in LGRBs the flare rise time $t_{\rm r}$ and decay time $t_{\rm d}$, like the w, linearly evolve with $t_{\rm pk}$ (Chincarini et al. 2010; Bernardini et al. 2011) preserving their ratio $t_{\rm r} \sim 0.5 t_{\rm d}$ over four decades in $t_{\rm pk}$ and leading to flares with asymmetry values very similar to the prompt pulses (while being a factor $\geq$100 wider).[13]

4.4 Flux contrast

While the $w(t_{\rm pk})$ and $\Delta t/t$ measurements do not allow us to distinguish a flare in a LGRB from a flare candidate in a SGRB[14], the flux contrast distributions $\Delta F/F$ of the two populations are significantly different (Fig. 7), with SGRB flare candidates having systematically *lower* $\Delta F/F$ values. In contrast to LGRBs, none of the ~60 *Swift* X-ray afterglows associated to SGRBs shows cases of powerful ($\Delta F/F \gg 5$), highly variable $\Delta t/t \ll 1$ flares. A *Chandra* observation of 9 X-ray photons from SGRB 050709[15] ~15 d after the explosion led Fox et al. (2005) to conclude the presence of high-amplitude ($\Delta F/F \approx 10$), fast variability ($\Delta t/t \approx 0.01$) in its X-ray afterglow. *Swift* observations suggest that this kind of variability, if present, is extremely rare. SGRBs lack the presence of prominent fast-rise exponential decay features superimposed over their X-ray afterglow for $t_{\rm pk}/(1+z) > 60$ s.

[13] Note that given the limited statistics of the SGRB X-ray afterglows, nothing can be said about the asymmetry of SGRB flare candidates.

[14] The limited number of flare candidates plays a role in this statement. We cannot exclude that a significant improvement of the SGRB and LGRB statistics could lead to the detection of secondary effects.

[15] GRB 050709 is a short burst detected by *HETE* for which *Swift* did not do the follow up. For this reason it is not included in the present sample. The episode of prominent variability is possibly related to a statistical fluctuation.

Lazzati et al. (2011) predicted that if flares in SGRBs originate from the intrinsic variability of their inner engine, their $\Delta F/F$ distribution should be analogous to the brighter population ($\Delta F/F \sim 100$) of LGRB flares. With a maximum $\Delta F/F \approx 2$ the detected SGRB flare candidates are *not* consistent with these expectations and populate instead the *low* end of the LGRB distribution unless the SGRB continuum flux F has been overestimated by a factor ~100 which we consider unlikely. An interesting possibility is that the X-ray light curves of SGRBs are dominated by an emission component which is *not* present in the LGRB afterglows (such as the EE): this would lead to systematically lower $\Delta F/F$ for SGRBs when compared to LGRB flares. The clustering of the $\Delta F/F$ ratio around 1 would suggest a link between flare candidates and underlying continuum. However, the strong correlation found by Nysewander et al. (2009) between the X-ray afterglow flux and prompt fluence of *both* long and short GRBs reveals a high degree of similarity between their X-ray afterglows at least at late times (i.e. 11 h, observer frame). A detailed comparison of short and long GRB X-ray afterglows at *early* times is in preparation.

The SGRB $\Delta F/F$ observed at $t_{\rm pk} \sim 100$ s is instead typical of LGRB flares detected at much later times: $t_{\rm pk} \gtrsim 1$ ks (Bernardini et al. 2011). From Fig. 9 it is apparent that SGRB flare candidates are consistent with the $\Delta F/F$ distribution of LGRB flares detected at the *same* $t_{\rm pk}/T_{90}$ epoch (where T_{90} is the duration of the prompt 15-150 keV emission): differences instead arise if we compare the properties of the two classes at the same $t_{\rm pk}/(1+z)$. While the T_{90} is possibly a crude estimation of the intrinsic time-scale of evolution of the central engine, this result opens the possibility that prominent fluctuations are not currently detected in SGRB afterglows because of the intrinsically late-time *Swift* repointings: $t_{\rm rep} \sim 100$ s corresponds to $t_{\rm rep}/T_{90} \sim 100$–1000 (SGRBs) and to $t_{\rm rep}/T_{90} \sim 1$–10 (LGRBs). From another perspective this finding directly connects the flux properties of SGRB flare candidates to the evolution time-scale of their central engines. The prompt T_{90} qualifies as a good proxy for the intrinsic time-scale that drives the subsequent flux evolution of flares and flare candidates in long and short GRBs, respectively. This conclusion is strengthened by the results of Section 4.5.

4.5 Energetics

4.5.1 Flare $L_{\rm pk}$ evolution with time

While SGRB prompt pulses compete with those of LGRBs in terms of peak luminosity, the same is not true for their late-time variability: SGRB flare candidates are a factor $\sim 10^2$ dimmer that expected (Fig. 3). Section 4.4 and Fig. 5 suggest that long and short GRBs might be astrophysical systems *evolving* on completely different time-scales and with different energy budgets but otherwise based on a similar physical mechanism of emission. In that case, we would expect the evolution of the flare luminosity to exhibit much better agreement between long and short GRBs once the intrinsic time-scale and central engine energy scaling are properly accounted for. Fig. 8 shows that this is indeed the case: long and short GRBs are consistent with a common (albeit highly scattered) $L_{\rm pk,F}/\langle L_{\rm P}\rangle \sim (t_{\rm pk}/T_{90})^{-0.9\,\pm 0.1}$ scaling (where $\langle L_{\rm P}\rangle$ and T_{90} are the average prompt luminosity and duration of each GRB in the 15-150 keV energy range, respectively). Fig. 8 therefore establishes a direct connection between the properties of SGRB flare candidates and LGRB flares, providing further support to a common, likely *internal* origin (see Section 4.7).

Downloaded from http://mnras.oxfordjournals.org/ at NASA Goddard Space Flight Ctr on July 11, 2014

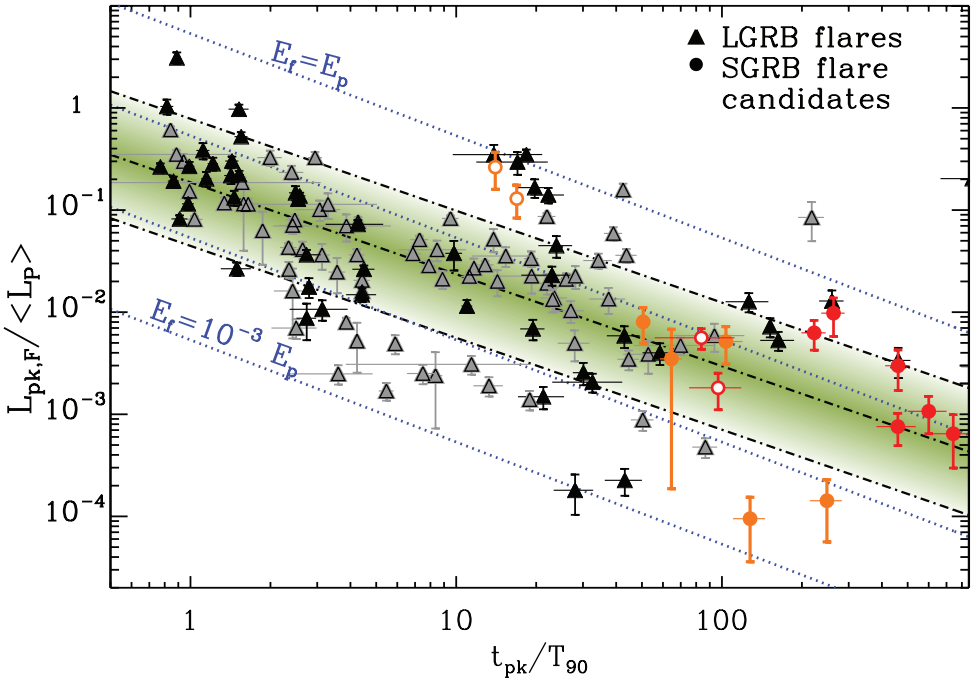

Figure 8. Renormalized peak luminosity versus renormalized peak time for the sample of LGRB flares from Chincarini et al. (2010) and Bernardini et al. (2011) (triangles) with $t_{pk}/T_{90} \lesssim 10^3$ and SGRB flare candidates (circles). Dark and light colours distinguish events with and without redshift measurement to allow a direct comparison with Fig. 3. Open symbols refer to SGRBs with detected extended emission. Black dot–dashed line: best-fitting power-law model for the LGRB sample: $L_{pk,F}/\langle L_P \rangle = 10^{-0.72\ \pm 0.03}(t_{pk}/T_{90})^{-0.9\ \pm 0.1}$ and extrinsic scatter $\sigma = 0.62 \pm 0.01$. The shaded area marks the $\pm 1\,\sigma$ region around the best fit. From top to bottom, the blue dotted lines mark the $E_{iso,F}/E_{iso,P} = 1, 0.1, 0.01, 0.001$ regions of the plane, where $E_{iso,F}$ and $E_{iso,P}$ have been calculated in the 0.3–10 and 15–150 keV energy bands, respectively. The flare width versus peak time relation from Chincarini et al. (2010) has been used.

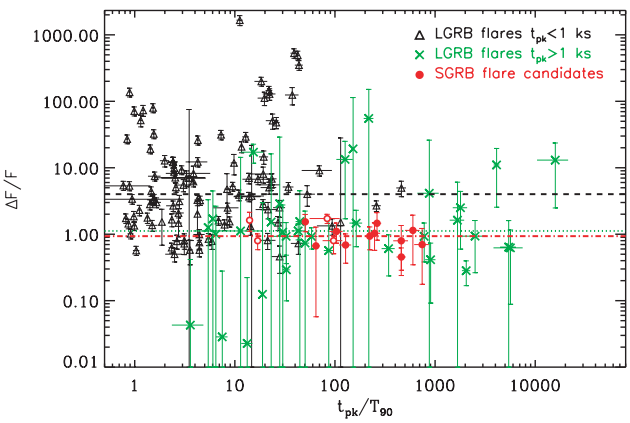

Figure 9. Relative variability flux $\Delta F/F$ evolution as a function of t_{pk}/T_{90}: black triangles and green stars indicate LGRB flares with $t_{pk} < 1$ ks (Chincarini et al. 2010) and $t_{pk} > 1$ ks (Bernardini et al. 2011), respectively. Red open and filled circles: flare candidates in SGRBs with and without extended emission, respectively. Horizontal dashed, dot and dot–dashed lines mark the $\Delta F/F$ median value for the three samples.

In the context of a one to one comparison of short versus long GRB X-ray variability, the renormalized peak luminosity and renormalized peak time are the most relevant quantities: the observed T_{90} and $\langle L_P \rangle$, with their sensitivity to the instrument threshold and energy band passes, likely provide crude (but nevertheless the best) approximations to the exact values to be used (while being partially responsible for the large scatter of the relation). In particular the loss of total fluence in the prompt γ-ray due to the limited *Swift*-BAT band-pass likely affects short more than long GRBs. As a result the SGRB $L_{pk,F}/\langle L_P \rangle$ values may be overestimated when compared to LGRB values[16]. However, Fig. 8 shows that even a factor of several of overestimation (Nysewander et al. 2009) would not strongly affect our conclusions.

4.5.2 *Implications of the $L_{pk,F}/\langle L_P \rangle$ versus t_{pk}/T_{90} relation*

SGRB flare candidates are consistent with the highly scattered $L_{pk,F}/\langle L_P \rangle$ versus t_{pk}/T_{90} relation established by LGRB flares: since the origin of LGRB flares is likely connected to their prompt pulses (Krimm et al. 2007; Margutti et al. 2010b), we speculate that a similar physical mechanism (except for its energy budget and lifetime) powers long and short GRBs: observationally speaking, the main distinction between flares and prompt emission in LGRBs is the evolution of the former with time for $t_{pk} > T_{90}$. It is therefore natural to expect a similar scaling of LGRB flares and SGRB flare candidates in terms of t_{pk}/T_{90} if they share a common origin.

A comparison of the prompt γ-ray emission of SGRBs to the initial 2 s of LGRBs reveals a high degree of similarity in the pulse duration distributions and correlations in the temporal structure of the two classes (Nakar & Piran 2002a; McBreen et al. 2001);[17] an analogous study was performed by Ghirlanda et al. (2009) in the spectral domain: based on the spectral analysis of the prompt emission of 79 short and 79 long GRBs detected by BATSE the authors

[16] This effects would mainly depend on the different prompt emission spectral peak energy E_{peak} of long and short GRBs: however, Ghirlanda et al. (2009) showed that SGRBs have a harder low-energy spectral component but only slightly higher E_{peak} when compared to LGRBs.

[17] The temporal evolution of pulses as a function of *frequency* (i.e. the spectral lag) shows however dissimilarities, as discussed in Section 4.6.

Downloaded from http://mnras.oxfordjournals.org/ at NASA Goddard Space Flight Ctr on July 11, 2014

showed that no difference is found comparing the spectral properties of SGRBs to the first 1–2 s emission of LGRBs. Temporal and spectral studies therefore point to a common mechanism operating in the first few seconds of any event. The present work extends this similarity to their late-time emission.

The quasi-linear $w(t_{\rm pk})$ evolution shared by long and short GRBs allows us to draw reference lines of equal flare-to-prompt energy ratios as a function of $t_{\rm pk}/T_{90}$ in the $L_{\rm pk,F}/\langle L_{\rm P}\rangle$ plane (blue dotted lines of Fig. 8). Flares in the 0.3–10 keV band pass are found to emit between (0.1 − 100) per cent of the prompt 15–150 keV $E_{\rm iso,P}$, with the majority of them lying between the 1 per cent and 10 per cent levels. Little evolution of the flare-to-prompt energy ratio $E_{\rm iso,F}/E_{\rm iso,P}$ in terms of $t_{\rm pk}/T_{90}$ can be inferred from the plot (for $t_{\rm pk}/T_{90} \lesssim 300$). In particular, SGRB flare candidates and LGRB flares show comparable flare-to-prompt energy ratios, as reported in Table 2. This finding provides further support to a physical link between LGRB flares and SGRB flare candidates.

The GRB central engines seem to release comparable fractions of prompt emission energy at late times, irrespective of the long or short GRB nature. From Fig. 8,

$$\frac{L_{\rm pk,F}}{\langle L_{\rm P}\rangle} = N_1 \left(\frac{t_{\rm pk}}{T_{90}}\right)^{-(1+\alpha)} \tag{1}$$

with $\alpha = -0.1 \pm 0.1$. The best-fitting rest-frame $w(t_{\rm pk})$ relation reads

$$\left(\frac{w}{1+z}\right) = N_2 \left(\frac{t_{\rm pk}}{1+z}\right)^{(\beta+1)} \tag{2}$$

with $\beta = 0.2 \pm 0.2$ (Fig. 2). Equations (1) and (2) express common properties of LGRB flares and SGRB flare candidates. The normalization parameters N_1 and N_2 possibly hide the dependence of $L_{\rm pk,F}/\langle L_{\rm P}\rangle$ and w on other parameters. This hidden dependence might be partially responsible for the large scatter of relation (1); α and β parametrize the *non*-linear dependence of $L_{\rm pk,F}/\langle L_{\rm P}\rangle$ and $w/(1+z)$ on $t_{\rm pk}/T_{90}$ and $t_{\rm pk}/(1+z)$, respectively. Combining equations (1) and (2) it is possible to show that

$$\frac{E_{\rm iso,F}}{E_{\rm iso,P}} = \mathcal{N} \left(\frac{t_{\rm pk}}{1+z}\right)^{\beta-\alpha} \left(\frac{T_{90}}{1+z}\right)^{\alpha}, \tag{3}$$

where $\mathcal{N} \sim 0.9^2 N_1 N_2$ and $E_{\rm iso,F} \sim 0.9 L_{\rm pk} w/(1+z)$ (valid for a Norris et al. 2005 flare profile where w is calculated between $1/e$ intensity points and with $t_{\rm r} = 0.5 t_{\rm d}$ as found by Chincarini et al. 2010 for LGRB flares). Equation (3) shows that $E_{\rm iso,F}/E_{\rm iso,P} \propto [t_{\rm pk}/(1+z)]^{\beta-\alpha}$: a weak dependence of the flare-to-prompt energy ratio on $t_{\rm pk}/(1+z)$ is expected *if* $\beta - \alpha \sim 0$. From the best-fitting relations, we find that both parameters are consistent with 0 at 1σ: in particular $\beta - \alpha = 0.3 \pm 0.2$ (consistent with 0 at $1.5\,\sigma$ level). At similar $t_{\rm pk}/(1+z)$ a residual dependence on the rest-frame prompt duration $T_{90}/(1+z)$ is expected to arise from the third term of equation (3): this dependence, if present, would be able to distinguish the population of LGRB flares from SGRB flare candidates detected at the same rest-frame peak time in terms of $E_{\rm iso,F}/E_{\rm iso,P}$. However, $\alpha = -0.1 \pm 0.1$ (and the relation is highly dispersed). We therefore conclude that the quasi-linear $w(t_{\rm pk})$ and $L_{\rm pk,F}/\langle L_{\rm P}\rangle$ versus $t_{\rm pk}/T_{90}$ relations translate into $E_{\rm iso,F}/E_{\rm iso,P}$ ratios which, at first order approximation, show limited dependence on both the properties of the central engine (i.e. duration of the prompt emission) and elapsed time from the explosion.

From Fig. 3, $L_{\rm pk,F}^{\rm SGRB}/L_{\rm pk,F}{}^{\rm LGRB} \sim 10^{-2}$ at the same $t_{\rm pk}/(1+z)$. A factor of ∼100 is roughly the ratio of the isotropic energy emitted by long and short GRBs during their *prompt* γ-ray emission (Fig. 5, inset).[18] LGRB flares and SGRB flare candidates are therefore expected to show a similar behaviour in the $L_{\rm pk,F}/E_{\rm iso,P}$ versus $t_{\rm pk}/(1+z)$ plane (in strict analogy with the X-ray afterglow scaling found by Nysewander et al. 2009, their fig. 6). Equation (1) can be easily re-arranged into

$$\frac{L_{\rm pk,F}}{E_{\rm iso,P}} = N_1 \left(\frac{t_{\rm pk}}{1+z}\right)^{-(\alpha+1)} \left(\frac{T_{90}}{1+z}\right)^{\alpha}. \tag{4}$$

Again, the limited departure of $L_{\rm pk,F}/\langle L_{\rm P}\rangle$ from a linear relation in $t_{\rm pk}/T_{90}$ ($\alpha = -0.1 \pm 0.1$) causes LGRB flares and SGRB flare candidates to share the same scaling (at least at first order approximation).

All the above indications point to a SGRB flare candidates internal origin (Section 4.7) and establish a connection between long and short GRB X-ray variability.

4.6 The lag–luminosity relation

Negligible spectral lag above ∼25 keV is the fundamental attribute that makes the prompt γ-ray emission of short bursts different from LGRBs, in addition to their narrower pulses, shorter duration and slightly harder emission (Norris & Bonnell 2006 and references therein). The spectral lag is the time difference between the arrival of high-energy and low-energy photons: in our analysis, a positive value indicates that high-energy photons lead the low-energy emission. During the prompt phase of LGRBs the spectral lag $\tau_{\rm lag}^{\gamma}$ is anti-correlated with the peak luminosity as shown in Fig. 6 (Norris, Marani & Bonnell 2000; Ukwatta et al. 2010); in contrast, short bursts have small $\tau_{\rm lag}^{\gamma}$ (Norris & Bonnell 2006) and occupy a separate area of the $L_{\rm pk}$ versus $\tau_{\rm lag}^{\gamma}/(1+z)$ parameter space (Fig. 6 and Gehrels et al. 2006). Recently, Margutti et al. (2010b) have demonstrated that, in strict analogy to their prompt pulses, LGRB X-ray flares define a lag–luminosity anti-correlation, where the lag is computed in the X-ray band (black dots of Fig. 6). With the present work we complete the observational picture above, showing that flare candidates in SGRBs fall off the lag–luminosity relation defined by LGRBs: this furthermore supports a robust connection between prompt pulses and flare candidates in short bursts. At the same time this result points to some differences between LGRB flares and SGRB flare candidates.

While SGRB prompt pulses are significantly narrower than LGRB pulses (Nakar & Piran 2002a; Nakar & Piran 2002b), flares show instead comparable width in both classes (Fig. 2). Hakkila et al. (2008) showed the existence of a lag-width correlation for prompt pulses: the wider the prompt pulse, the longer the lag. This behaviour has been recently extended to LGRB flares by Margutti et al. (2010b). The similar width of LGRB flares and SGRB flare candidates implies that the lag-width relation cannot be invoked to explain the lag of SGRB flare candidates which are systematically shorter than expected from the lag–luminosity relation of LGRB flares.

The physical cause of lags in the GRBs prompt emission is not yet understood: variations in the line-of-sight (Salmonson 2000); variations of the off-axis angle (Ioka & Nakamura 2001) and rapid radiation cooling effects (Schaefer 2004) are a few of the proposed models. In particular it is at the moment unclear if lags in short bursts

[18] Note that the same ∼100 factor is found as the ratio of the isotropic energy emitted by LGRB *flares* and SGRB *flare* candidates: this is a direct consequence of their flare peak luminosity ratio $L_{\rm pk}^{\rm SGRB}/L_{\rm pk}{}^{\rm LGRB} \sim 10^{-2}$, coupled to the very similar $w(t_{\rm pk})$ evolution.

© 2011 The Authors, MNRAS **417,** 2144–2160
Monthly Notices of the Royal Astronomical Society © 2011 RAS

Downloaded from http://mnras.oxfordjournals.org/ at NASA Goddard Space Flight Ctr on July 11, 2014

are small and non-measurable or intrinsically zero. According to the first possibility short and long GRBs would be powered by a similar, progenitor-independent physical mechanism, with SGRBs being faster evolving versions of LGRBs. The latter would instead point to some intrinsic differences. At present it is not possible to observationally distinguish between the two scenarios.[19]

In the case of flares, the situation is complicated by the limited and fixed energy band-passes used for the lag calculation (0.3–1 versus 3–10 keV). The fundamental origin of the observed lag is the spectral evolution of a pulse (or flare) profile to lower energies (Kocevski & Liang 2003; Margutti et al. 2010b). The spectral peak energy $E_{\rm peak}$ decrease in time plays a major role in determining the observed spectral evolution and lag value (see Margutti et al. 2010b for details). As a consequence, if the observed $E_{\rm peak}$ does not cross the instrumental band pass during the emission, a limited spectral evolution will be detected and a short time lag determined. The shorter (when compared to what expected from the LGRB flare lag–luminosity relation) time lag of SGRB flare candidates might be partially a consequence of this observational effect (while possibly being intrinsically larger):[20] the results from Sections 4.4 and 4.5 suggest that long and short bursts basically differ in the intrinsic time-scale of central engine evolution (with SGRBs evolving faster). Since for LGRBs $E_{\rm peak,F}^{\rm LGRB}/E_{\rm peak,P}^{\rm LGRB} \lesssim 0.01$ (with $E_{\rm peak,F}^{\rm LGRB} \sim 1-3$ keV, observed value, Margutti et al. 2010b), the faster evolution of short bursts likely implies $E_{\rm peak,F}^{\rm SGRB}/E_{\rm peak,P}^{\rm SGRB} \ll 0.01$ for flares detected at the same observed $t_{\rm pk}$. This result translates into: $E_{\rm peak,F}^{\rm SGRB} < 1$ keV considering that $E_{\rm peak,P}^{\rm SGRB} \sim E_{\rm peak,P}{}^{\rm LGRB}$ as order of magnitude estimation (Ghirlanda et al. 2009). According to this scenario, $E_{\rm peak,F}^{\rm SGRB}$ is below the XRT band for the majority of the emission, possibly leading to a lag underestimation. The presence of this observational bias makes the interpretation of the entire lag–luminosity relation far from being straightforward. We stress that the dependence of the lag–luminosity on the choice of the fixed energy bands (both in the rest frame and in the observer frame) should be removed before addressing the physical interpretation of the anti-correlation. However, this topic goes beyond the scope of this paper and will be addressed in a future work.

With this caveat in mind we note that if the energy $E_{\rm iso,F}$ released by flares at different $t_{\rm pk}$ is similar (as indicated by Section 4.5), then, considering that $L_{\rm pk,F} \sim E_{\rm iso,F}/w$ with the lag being positively correlated to the w (Margutti et al. 2010b), we would expect $L_{\rm pk,F}$ to be anti-correlated with $\tau_{\rm lag}^{x}$ as observed for LGRB flares of Fig. 6: $L_{\rm pk,F} = N_{\rm lag}^{\rm F}(\tau_{\rm lag}^{x})^{-1}$. In particular the normalization $N_{\rm lag} \propto E_{\rm iso,F}$, which implies $N_{\rm lag}^{\rm LGRB} \sim 100 N_{\rm lag}^{\rm SGRB}$ (since $E_{\rm iso,F}^{\rm LGRB} \sim 100\, E_{\rm iso,F}{}^{\rm SGRB}$, Table 2). This simple argument predicts the SGRB flare candidates to be off the LGRB flare lag–luminosity relation of a factor $\gtrsim 100$ as observed (the $\gtrsim$ inequality accounts for the possible underestimation of the real lag due to the fixed and limited energy band-passes bias of the previous paragraph). This finding would support the presence of non-measurable (but still *non-zero*) lags for the short burst prompt emission.

4.7 The flare candidates internal origin

The above indications point to a link between the properties of flare candidates and prompt pulses in SGRBs (for LGRBs this was demonstrated by Margutti et al. 2010b). This result would naturally arise if both kind of emission share a common origin: we refer to this possibility as the *internal origin* interpretation. Theoretical models consistent with this picture can be divided into two categories: models requiring a late-time GRB central engine activity and models where the central engine is *not* required to be active at the time of the flare detection.

The second class of models includes the magnetic reconnection interpretation (Lyutikov & Blandford 2003; Giannios 2006): flares would originate from residual, late-time magnetic reconnection events within the original outflow (the *same* ejecta powered the prompt phase) triggered by its deceleration due to the sweeping-up of the external medium. The deceleration of the original ejecta during the afterglow phase causes an increase in the size of causally connected regions, thus enabling reconnection of increasingly larger magnetic structures. The smooth continuum would be instead afterglow emission from the shocked external medium.

Alternatively, flares and prompt pulses would automatically share a set of observational properties if they both directly arise from the GRB central engine activity (first class of models above). If this is the case, the central engine would be active on much longer time-scales than previously thought (see e.g. Perna et al. 2006; Rosswog 2007; Lee et al. 2009); at the same time, the similarity of LGRB flares and SGRB flare candidates in the $L_{\rm pk}/\langle L\rangle$ versus $t_{\rm pk}/T_{90}$ plane as well as in the $\Delta F/F$ versus $t_{\rm pk}/T_{90}$ space would point to a similar late time evolution of long and short GRB central engines.

It is not possible to observationally discriminate between the two scenarios using the present set of data. Careful modelling is required (Margutti et al., in preparation).

5 CONCLUSIONS

This work presents the first comprehensive analysis of flare candidates in SGRBs and provides a comparison to the observational properties of X-ray flares in LGRBs with the aim to draw an observational picture of SGRB X-ray variability *any* theoretical model is required to explain.

Our analysis shows that the origin of the SGRB X-ray light-curve variability is independent from the large-scale host galaxy environment and is not correlated to the detected afterglow lifetime. We find that flare candidates appear in different types of SGRB host galaxy environments and show no clear correlation with the X-ray afterglow lifetime; flare candidates are detected both in SGRBs with a bright extended emission (EE) in the soft γ-rays and in SGRBs which do not show such component (Section 4.2). We cannot exclude that flare candidates originate on top of faint (and undetected in the γ-rays) EEs. In particular, SGRB flare candidates are consistent with being drawn from the LGRB flare population when considering:

(1) The flare to prompt energy ration $E_{\rm iso,F}/E_{\rm iso,P}$ (Fig. 5, Section 4.5);

(2) The relative variability time-scale $\Delta t/t < 1$ (Fig. 7, Section 4.3);

[19] From the prompt lag-width relation of Hakkila et al. (2008): $\tau^{\gamma,\rm LGRB}/w_{\rm P}^{\rm LGRB} \sim 0.01$–$0.1$. Using $w_{\rm P}^{\rm SGRB} \sim 0.05$ s as typical value from Nakar & Piran (2002b), we have $\tau^{\gamma,\rm SGRB} \sim 0.5-5$ ms assuming that the $\tau^{\gamma}/w_{\rm P}$ ratio is universal. We typically resolve lags in SGRBs with a sensitivity of a few ms. This implies that we would be barely able to measure lags in the SGRB prompt pulses even if SGRBs were to follow the LGRB $\tau^{\gamma}/w_{\rm P}$ relation.

[20] Note that the limited brightness of the flare candidates compared to the underlying X-ray continuum does not allow us to perform a one-to-one comparison with the spectral properties of LGRB flares to quantitatively check this possibility.

Downloaded from http://mnras.oxfordjournals.org/ at NASA Goddard Space Flight Ctr on July 11, 2014

(3) The rest-frame flare width evolution with time $w(t_{\rm pk})$ (Fig. 2, Section 4.3).

(4) The hard-to-soft trend of the emitted radiation (see e.g. Fig. 1).

The main parameter driving the duration of the episodes of variability is the elapsed time from the explosion, with very limited dependence on the different progenitors, environments, lifetimes, prompt variability time scales and energy budgets. The origin of the flare $w(t_{\rm pk})$ relation must arise from what is in common for the long and short burst models. From another perspective this result implies that for $t_{\rm pk} > 100$ s the flare duration is likely to retain no memory of the variability time-scales of the original prompt mechanism at work. This would explain why the flare to prompt pulse width ratio is different for long and short GRBs.

On the contrary, SGRB flare candidates significantly differ from the standard X-ray flare emission observed in LGRBs at the same $t_{\rm pk}/(1+z)$ in terms of:

(5) Peak luminosity $L_{\rm pk,F}^{\rm SGRB} \sim 0.01 L_{\rm pk,F}^{\rm LGRB}$ (Figs 3 and 4, Section 4.5);

(6) Isotropic energy $E_{\rm iso,F}^{\rm SGRB} \sim 0.01 E_{\rm iso,F}^{\rm LGRB}$ (Fig. 5, Section 4.5);

(7) Flare to prompt luminosity ratio $L_{\rm pk,F}/L_{\rm pk,P}$. Flare candidates in SGRBs are ∼100 times dimmer than in LGRB;

(8) Relative variability flux $\Delta F/F$ (Fig. 7): we find $\Delta F/F \sim 1$ for all SGRB flare candidates (Section 4.4);

(9) Lag–luminosity relation: like SGRB prompt pulses, flare candidates show shorter lags than expected from the lag–luminosity relation of LGRB flares (Fig. 6, Section 4.6).

However and more importantly, the differences listed at points (5), (6), (7) and (8) above disappear once the different time-scale of evolution of the long and short GRB central engine as well as the different energy scaling of the two systems is properly accounted for (Fig. 8, Sections 4.5.1 and 4.5.2). This finding provides a connection between the properties of the detected SGRB X-ray light-curve variability and LGRB flares, suggesting a common, *internal* origin. As a result, we conclude that similar dissipation and/or emission mechanisms are likely to be responsible for the prompt and flare emission in long and short GRBs, with SGRBs being less energetic albeit faster evolving versions of the long category.

ACKNOWLEDGMENTS

We thank the anonymous referee for helpful suggestions that improved the quality of this work. RM thanks Lorenzo Amati for sharing his data before publication. This work is supported by ASI grant SWIFT I/011/07/0, by the Ministry of University and Research of Italy (PRIN MIUR 2007TNYZXL), by MAE (Ministry of Exterior), by the University of Milano Bicocca, Italy and by the ERC advanced research grant 'GRBs'.

REFERENCES

Barthelmy S. D. et al., 2005a, Space Sci. Rev., 120, 143
Barthelmy S. D. et al., 2005b, Nat, 439, 994
Berger E., 2011, New Astron. Rev., 55, 1
Bernardini M. G., Margutti R., Chincarini G., Guidorzi C., Mao J., 2011, A&A, 526, 27
Burrows D. N. et al., 2005, Space Sci. Rev., 120, 165
Campana S. et al., 2006, A&A, 454, 113
Chincarini G. et al., 2010, MNRAS, 406, 2113
D'Avanzo P. et al., 2009, A&A, 498, 711
Dermer C., 2008, ApJ, 684, 430
Eichler D., Livio M., Piran T., Schramm D. N., 1989, Nat, 340, 126
Evans P. et al., 2010, A&A, 519, 102
Fong W. F., Berger E., Fox D. B., 2010, ApJ, 708, 9
Fong W. F. et al., 2011, ApJ, 730, 26
Fox D. B. et al., 2005, Nat, 437, 845
Fruchter A. S. et al., 2006, Nat, 441, 463
Gehrels N. et al., 2004, ApJ, 611, 1005
Gehrels N. et al., 2006, Nat, 444, 1044
Ghirlanda G., 2010, in Comastric A., Angelini L., Cappi M., eds, AIP Conf. Proc. Vol. 1248, X-ray Astronomy 2009: Present Status, Multi-Wavelength Approach and Future Perspectives. Am. Inst. Phys., Melville, p. 51
Ghirlanda G., Nava L., Ghisellini G., Celotti A., Firmani C., 2009, A&A, 496, 585
Giannios D., 2006, A&A, 455, L5
Goad M. R. et al., 2007, A&A, 468, 103
Granot J., Nakar E., Piran T., 2003, Nat, 426, 138
Grupe D. et al., 2006, ApJ, 653, 462
Hakkila J., Preece R. D., 2011, ApJ, submitted (arXiv:1103.5434)
Hakkila J., Giblin T. W., Norris J. P., Fragile P. C., Bonnell J. T., 2008, ApJ, 677, L81
Ioka K., Nakamura T., 2001, ApJ, 554, L163
Ioka K. et al., 2005, ApJ, 631, 429
Kocevski D., Liang E., 2003, ApJ, 594, 385
Kouveliotou C. et al., 1993, ApJ, 413, L101
Krimm H. A. et al., 2007, ApJ, 668, L147
Kulkarni S. R. et al., 1998, Nat, 395, 663
Kumar P., Piran T., 2000a, ApJ, 532, 286
Kumar P., Piran T., 2000b, ApJ, 535, 152
La Parola V. et al., 2006, A&A, 454, 753
Lazzati D., Morsnony B. J., Begelman M. C., 2010, MNRAS, 717, 239
Lazzati D., Blackwell C. H., Morsnony B. J., Begelman M. C., 2011, MNRAS, 411, L16
Lee W. H., Ramirez-Ruiz E., L-pez-Cmara D., 2009, ApJ, 699, L93
Lyutikov M., Blandford R., 2003, preprint (astro-ph/0312347)
McBreen S., Quilligan F., McBreen B., Hanlon L., Watson D., 2001, A&A, 380, L31
MacFadyen A. I., Woosley S. E., 1999, ApJ, 524, 262
Malesani D. et al., 2007, A&A, 473, 77
Margutti R. et al., 2010a, MNRAS, 402, 46
Margutti R., Guidorzi C., Chincarini G., Bernardini M. G., Genet F., Mao J., Pasotti F., 2010b, MNRAS, 406, 2149
Margutti R. et al., 2011, MNRAS, 410, 1064
Markwardt C. B. et al., 2010, GCN Circular, 11111
Nakar E., 2007, Phys. Rep., 442, 166
Nakar E., Oren Y., 2004, ApJ, 602, L97
Nakar E., Piran T., 2002a, MNRAS, 330, 920
Nakar E., Piran T., 2002b, MNRAS, 331, 40
Narayan R., Paczynski B., Piran T., 1992, ApJ, 395, L83
Nava L., Ghirlanda G., Ghisellini G., Firmani C., 2008, MNRAS, 391, 639
Norris J. P., Bonnell J. T., 2006, ApJ, 643, 266
Norris J. P., Marani G. F., Bonnell J. T., 2000, ApJ, 534, 248
Norris J. P., Bonnell J. T., Kazanas D., Scargle J. D., Hakkila J., Giblin T. W., 2005, ApJ, 627, 324
Norris J. P., Gehrels N., Scargle J. D., 2010a, ApJ, 717, 411
Norris J. P., Ukwatta T. N., Barthelmy S. D., Gehrels N., Stamatikos M., Sakamoto T., 2010b, GCN Circular, 11113
Norris J. P., Gehrels N., Scargle J. D., 2011, ApJ, 735, 23
Nysewander M., Fruchter A. S., Pe'er A., 2009, ApJ, 701, 824
Paczynski B., 1986, ApJ, 308, L43
Panaitescu A., 2006, MNRAS, 367, L42
Perley D. et al., 2009, ApJ, 696, 1871
Perna R., Armitage J. P., Zhang B., 2006, ApJ, 636, L29
Piran T., 2004, Rev. Modern Phys., 76, 1143
Proga D., Zhang B., 2006, MNRAS, 370, L61
Rezzolla L., Giacomazzo B., Baiotti L., Granot J., Kouveliotou C., Aloy M. A., 2011, ApJ, 732, L6

Downloaded from http://mnras.oxfordjournals.org/ at NASA Goddard Space Flight Ctr on July 11, 2014

Romano P. et al., 2006, A&A, 456, 917
Rosswog S., 2007, MNRAS, 376, L48
Sakamoto T., Gehrels N., 2009, in Meegan C., Kauveliotou C., Gehrels C., eds, AIP Conf. Proc. Vol. 1133, Gamma-ray Burst: Sixth Huntsville Symposium. Am. Inst. Phys., New York, p. 112
Salmonson J. D., 2000, ApJ, 544, L115
Schaefer B. E., 2004, ApJ, 602, 306
Stamatikos M. et al., 2009, in Meegan C., Kauveliotou C., Gehrels C., eds, AIP Conf. Proc. Vol. 1133, Gamma-ray Burst: Sixth Huntsville Symposium. Am. Inst. Phys., New York, p. 356
Stanek K. Z. et al., 2003, ApJ, 591, L17
Troja E., Rosswog S., Gehrels N., 2010, ApJ, 723, 1711
Ukwatta T. N. et al., 2010, ApJ, 711, 1073
Vaughan S. et al., 2006, ApJ, 638, 920
Vlasis A., van Eerten H. J., Meliani Z., Keppens R., 2011, MNRAS, 415, 279
Zhang B. et al., 2006, ApJ, 642, 354

APPENDIX A: SGRB FLARES: TABLE

Table A1. Best-fitting parameters of SGRB flare candidates. From left to right: GRB, redshift; start time (t_s), amplitude (A) and shape parameters (τ_1, τ_2) of the best-fitting Norris et al. (2005) profile; width evaluated between $1/e$ intensity points; peak time (t_{pk}); relative variability time-scale ($\Delta t/t \equiv w/t_{pk}$); relative variability flux $\Delta F/F$: the value F is computed from the best fit of the continuous emission underlying the flare candidates (black solid line of Fig. 1); isotropic equivalent peak luminosity (L_{peak}) and energy (E_{iso}) computed in the 0.3–10 keV observer frame energy band.

GRB	z	t_s (s)	A (counts s^{-1})	τ_1 (s)	τ_2 (s)	w (s)	t_{pk} (s)	$\Delta t/t$	$\Delta F/F$	$L^{SGRB}_{pk,F}$ (10^{47} erg s^{-1})	$E^{SGRB}_{iso,F}$ (10^{48} erg)
050724	0.258	230.0	12.29 ± 0.88	12.40 ± 3.00	35.50 ± 4.20	65.11 ± 4.64	250.98 ± 1.80	0.26 ± 0.03	1.72 ± 0.27	1.49 ± 0.34	7.16 ± 1.98
051210	–	107.0	5.70 ± 1.60	430.00 ± 220.00	1.77 ± 0.87	14.09 ± 3.52	134.59 ± 1.43	0.10 ± 0.03	1.10 ± 0.37	–	–
051227	–	105.0	12.20 ± 2.10	8.90 ± 3.70	5.90 ± 1.70	14.35 ± 2.36	112.25 ± 0.88	0.13 ± 0.02	1.62 ± 0.52	–	–
051227	–	122.0	6.00 ± 0.00	10.00 ± 0.00	17.40 ± 2.50	34.94 ± 4.13	135.19 ± 0.96	0.26 ± 0.03	0.80 ± 0.21	–	–
060313	–	105.0	2.80 ± 1.20	19.00 ± 23.00	4.70 ± 5.30	14.13 ± 8.87	94.45 ± 2.21	0.15 ± 0.09	0.69 ± 0.32	–	–
060313	–	150.0	4.20 ± 1.70	111.00 ± 80.00	10.30 ± 7.10	38.72 ± 14.65	183.81 ± 4.50	0.21 ± 0.08	1.03 ± 0.46	–	–
070724A	0.457	75.0	7.80 ± 1.70	25.00 ± 23.00	7.80 ± 9.00	22.28 ± 15.76	88.96 ± 2.68	0.25 ± 0.18	0.93 ± 0.35	3.64 ± 1.18	5.07 ± 1.64
070724A	0.457	90.0	12.20 ± 3.90	42.00 ± 21.00	5.50 ± 2.10	19.10 ± 3.60	105.20 ± 1.26	0.18 ± 0.03	1.46 ± 0.65	5.68 ± 2.32	6.72 ± 2.75
070724A	0.457	150.0	3.79 ± 0.77	27.00 ± 17.00	43.00 ± 18.00	87.80 ± 21.55	184.07 ± 6.34	0.48 ± 0.12	0.45 ± 0.17	1.73 ± 0.74	9.73 ± 4.16
071227	0.383	150.0	4.36 ± 0.94	80.00 ± 41.00	7.30 ± 3.00	27.55 ± 5.74	174.17 ± 2.36	0.16 ± 0.03	0.80 ± 0.29	1.13 ± 0.44	2.03 ± 0.79
090607	–	89.0	7.60 ± 1.10	53.00 ± 31.00	14.00 ± 12.00	41.49 ± 22.22	116.24 ± 4.84	0.36 ± 0.19	1.54 ± 0.45	–	–
090607	–	122.0	3.30 ± 2.90	18.00 ± 17.00	39.00 ± 16.00	75.19 ± 25.52	148.49 ± 12.73	0.51 ± 0.18	0.67 ± 0.61	–	–
100117A	0.920	130.0	4.90 ± 0.73	2.00 ± 1.80	30.00 ± 0.00	42.77 ± 4.98	137.75 ± 3.55	0.31 ± 0.04	0.80 ± 0.56	9.97 ± 3.48	21.43 ± 7.48
100117A	0.920	164.0	7.03 ± 0.94	6.00 ± 0.00	42.90 ± 6.80	67.78 ± 9.13	180.04 ± 1.27	0.38 ± 0.05	1.14 ± 0.79	14.09 ± 5.60	47.45 ± 18.86
100117A	0.920	200.0	4.30 ± 1.30	101.00 ± 77.00	5.10 ± 3.50	22.11 ± 7.86	222.70 ± 2.57	0.10 ± 0.04	0.70 ± 0.52	8.49 ± 4.57	8.78 ± 4.73

APPENDIX B: SGRB FLARES: PLOTS

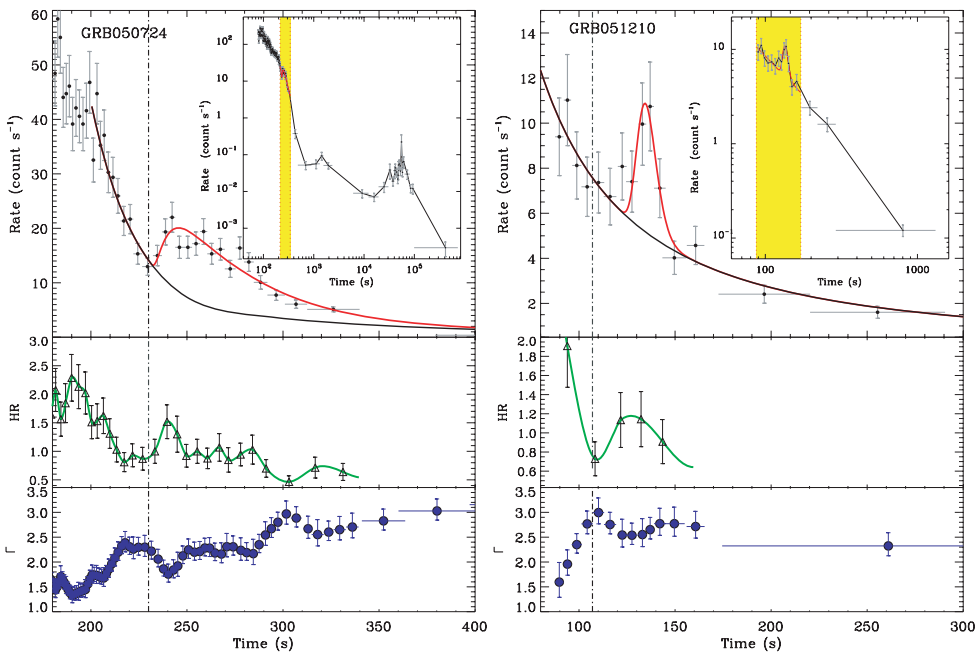

Figure B1. 0.3–10 keV count-rate light curve of GRB 050724 and GRB 051210. Black solid line: continuous X-ray emission underlying the flare candidates computed as described in Section 2.2; dashed lines: best-fitting flare candidate emission; red solid line: best estimate of the total emission. The vertical dot–dashed lines mark the flare candidate onset times. Inset: complete *Swift*-XRT light curve. The yellow filled area marks the time window for the computation of the CCF lag. Middle panels: HR evolution with time; the HR is computed between 1.5–10 (hard band) and 0.3–1.5 keV (soft band). Lower panels: spectral photon index evolution with time as computed by Evans et al. (2010).

Downloaded from http://mnras.oxfordjournals.org/ at NASA Goddard Space Flight Ctr on July 11, 2014

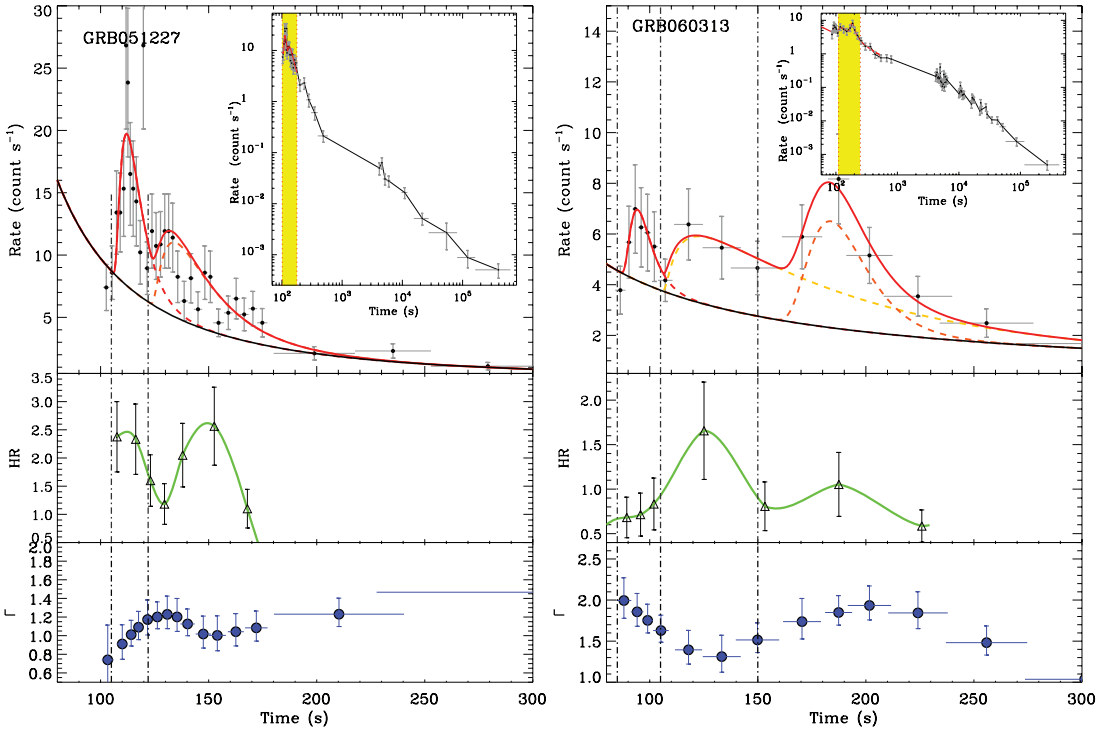

Figure B2. Same as Fig. B1 for GRB 051227 and GRB 060313.

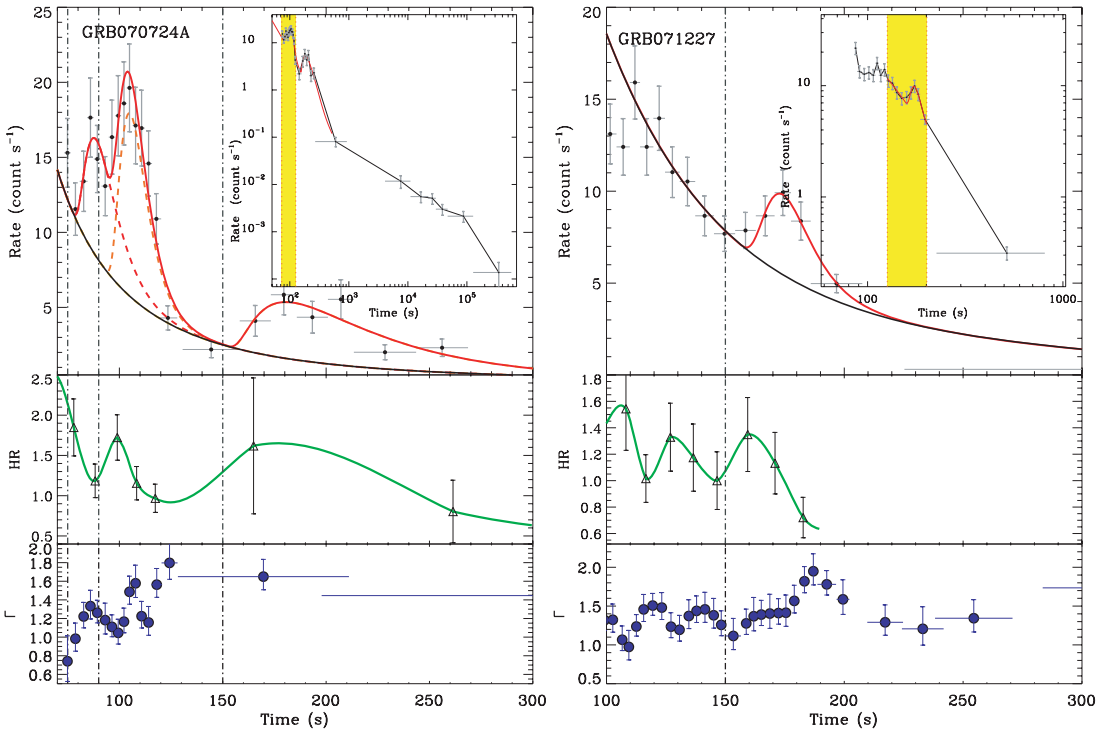

Figure B3. Same as Fig. B1 for GRB 070724A and GRB 071227.

Downloaded from http://mnras.oxfordjournals.org/ at NASA Goddard Space Flight Ctr on July 11, 2014

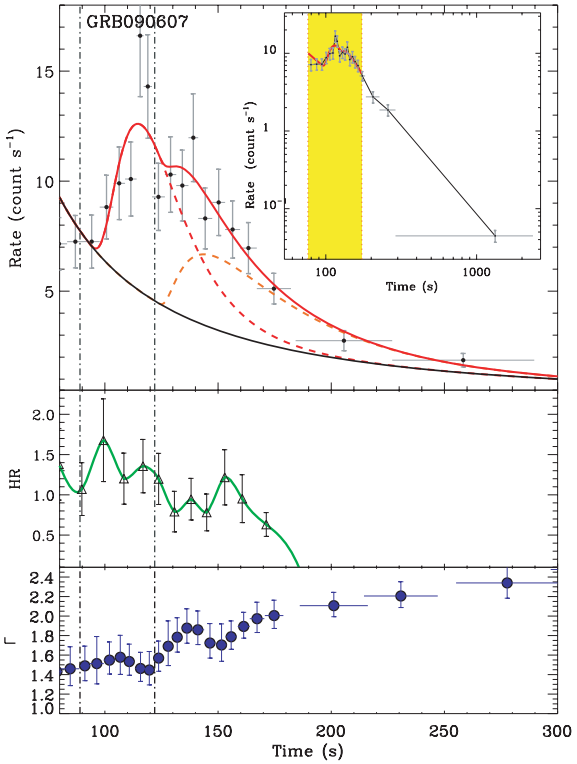

Figure B4. Same as Fig. B1 for GRB 090607.

This paper has been typeset from a TEX/LATEX file prepared by the author.

Downloaded from http://mnras.oxfordjournals.org/ at NASA Goddard Space Flight Ctr on July 11, 2014